

This is to certify that the

thesis entitled

CRACK PROPAGATION IN

Lif BICRYSTALS

presented by

JONG YEON LEE

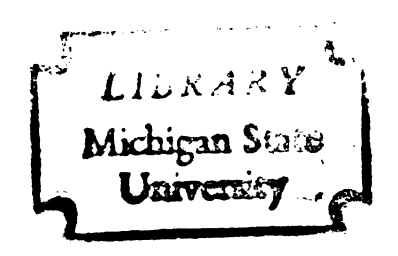
has been accepted towards fulfillment of the requirements for

Master of Science degree in Materials Science

Major professor

Date may 20,82.

O-7639





RETURNING MATERIALS:
Place in book drop to remove this checkout from your record. FINES will be charged if book is returned after the date stamped below.

CRACK PROPAGATION

IN

LITHIUM FLUORIDE BICRYSTALS

Ву

Jong Yeon Lee

A THESIS

Submitted to
Michigan State University
in partial fulfillment of the requirements
for the degree of

MASTER OF SCIENCE

Department of Metallurgy, Mechanics and Materials Science

ABSTRACT

CRACK PROPAGATION IN LITHIUM FLUORIDE BICRYSTALS

BY

Jong Yeon Lee

The role of relative crystallographic orientation and grain boundary orientation on crack propagation in LiF bicrystals was studied experimentally. LiF bicrystals were grown by Czochralski method with two single crystal seeds. Constant complience specimens were fractured by driving a wedge through notched specimens. Crack paths were observed by optical microscope, and fracture loads were measured using a load cell. Distribution of dislocations in the fracture surface was studied by etching the fracture surface. Crack paths and fracture loads were analyzed as a function of the misorientation angles. The direction of crack propagation was dictated according to the misorientation angles, and the fracture loads were increased as the misorientation angles increased. Cleavage steps were formed in the adjacent grain boundary. Although the relative crystallographic misorientation angles are different from specimen to specimen, the crack front speed decreases slightly as it approaches the grain boundary as is evidenced by the uniform density of dislocation etch pits throught the fracture surfaces.

ACKNOWLEDGEMENTS

The author wishes to express his deepest appreciation to his advisor, Dr. Karatholuvu N. Subramanian for his suggestions and guidance in this work.

The entire staff of the Department of Metallurgy,
Mechanics and Materials Science are thanked for their
assistance and helpful discussions.

Finally, to his wife and son, the author expresses his deep gratitude for their patience and encouragement.

TABLE OF CONTENTS

				Page
LIST	OF	TABI	CES	v
LIST	OF	FIG	JRES	vi
CHAP	rer			
1	1	INTRO	DDUCTION	1
		1.1	Advantages of Lithium Fluoride	1
		1.2	Theory of Fracture	2
2	(CRYS	TALLOGRAPHY	9
	:	2.1	Crystal Structure of LiF	9
	:	2.2	Deformation Behavior of LiF single	
			Crystal	11
	:	2.3	Fracture Behavior of LiF Single Crystal.	12
			2.3.1 Crack Nucleation	12
			2.3.2 Crack Growth and Propagation	15
3	(GRAII	N BOUNDARY	19
	;	3.1	Role of Grain Boundary in Deformation	19
	:	3.2	Role of Grain Boundary in Fracture	24
4	1	EXPE	RIMENTAL PROCEDURE	26
		4.1	Bicrystal Growth	26
		4.2	Specimen Preparation	30
		4.3	Test Fixture	32

TABLE OF CONTENTS -- continued

CHAPTER	ER		
	4.4	Test Procedure	34
5	RESU	LTS	35
	5.1	Measurement of Misorientation Angles	35
	5.2	Measurement of Fracture Loads	36
	5.3	Fracture Surface Studies	36
6	DISC	USSION	56
	6.1	Seed Setting	56
	6.2	Specimen Geometry	56
	6.3	Direction of Crack Propagation	60
	6.4	Relation Between Fracture Load and	
		Misorientation Angles	73
	6.5	Dislocation Etch Pit Studies	73
7	CONC	LUSIONS	83
REFE	ERENC	ES	85

LIST OF TABLES

TABLE	Page
l Velocity of propagation of brittle fra	acture 4
2 Chemical composition of LiF powder	27
3 Fracture mode and fracture load for va	arious θ
and 	38
4 Experimental values of surface energy.	
5 Calculated values of theoretical stren	ngth 65
6 Comparison of fracture load with 0 val	lues
$(86^{\circ} \le \phi \le 87^{\circ}, \text{ intercrystalline fract})$	ture) 75
7 Comparison of fracture load with θ val	lues
$(80^{\circ} \le \phi \le 82^{\circ}, \text{ intercrystalline fract})$	ture) 76
8 Comparison of fracture load with \$\phi\$ val	lues
$(86^{\circ} \le \theta \le 90^{\circ}, \text{ transcrystalline fract})$	ture) 77
9 Comparison of fracture load with \$\phi\$ val	lues
$(83^{\circ} < \theta < 85^{\circ}, \text{ transcrystalline fract})$	ture) 78

LIST OF FIGURES

FIGURE	Page
l Schematic diagram of crack formation at a	
grain boundary	6
2 Crystal structure of lithium fluoride	10
3 Crack nucleation by dislocation interaction	n 13
4 (a) Coordinate axes in two adjacent phases	•
(b) Relationship between the two system of	
coordinates	20
5 Passage of a dislocation from one crystal	into
the other	22
6 Czochralski furnace for growing LiF bicrys	tals 28
7 Specimen geometry	31
8 Test fixture for fracture load measurement	33
9 Transcrystalline crack propagation along t	he
primary cleavage plane	40
10 Transcrystalline crack propagation along t	he
primary cleavage plane	41
ll Transcrystalline crack propagation along t	he
primary cleavage plane	42
12 Transcrystalline crack propagation along t	he
primary cleavage plane	43
13 Transcrystalline crack propagation along t	he
secondary cleavage plane	44

		Page
14	Intercrystalline crack propagation	45
15	Intercrystalline crack propagation	46
16	Crack path branching (primary and secondary	
	cleavage)	47
17	Cleavage steps formed by the crack passage	
	through grain boundary	48
18	Cleavage steps formed by the crack passage	
	through grain boundary	49
19	Cleavage steps formed by the crack passage	
	through grain boundary	50
20	Slip lines formed by crack propagation	51
21	Uniform distribution of dislocation etch pits.	52
22	Uniform distribution of dislocation etch pits.	53
23	Uniform distribution of dislocation etch pits.	54
24	Uniform distribution of dislocation etch pits.	55
25	Parallel seed setting (tilt: 0°, twist: \$)	
	(a) Schematic drawing (b) Top view	57
26	45° slant seed setting (tilt: 45°, twist: \$\phi\$)	
	(a) Schematic drawing (b) Top view	58
27	Specimen geometry for three point bending test	
	to determine fracture surface energy	63
28	Locus of critical angles for intercrystalline	
	fracture and primary cleavage	69
29	Locus of critical angles for intercrystalline	
	fracture and secondary cleavage	70

		Page
30	Locus of critical angles for primary cleavage	
	and secondary cleavage	71
31	Crack propagation mode for various θ and ϕ .	
	Experimental points are indicated in the same	
	plot	72
32	Relation between fracture load and θ values	
	$(86^{\circ} \leq \phi \leq 87^{\circ}) \dots$	79
33	Relation between fracture load and θ values	
	$(80^{\circ} \leq \phi \leq 82^{\circ})$	80
34	Relation between fracture load and ϕ values	
	$(86^{\circ} \leq \theta \leq 90^{\circ}) \dots$	81
35	Relation between fracture load and ϕ values	
	(83 ⁰ < 8 < 85 ⁰)	82

1 INTRODUCTION

In crystalline materials, fracture may occur by either of two modes: transcrystalline cleavage or intercrystalline fracture. Sometimes, intercrystalline fracture indicates the presence of impurities segregated at the grain boundaries, or the presence of thin films of a second phase between the grains. In addition, there are many other factors that affect the fracture mode such as temperature, loading method, grain size, crystal structure, alloying elements, testing environment, and relative crystallographic orientation, etc.

In this work the role of relative crystallographic orientation, and grain boundary orientation with respect to crack path, on fracture was studied to gain a better understanding of the fundamental mechanism of crack propagation. For the experiment, LiF crystal was chosen because it has a simple crystal structure, well defined slip systems and cleavage planes; it is very resistant to atmospheric corrosion and is transparent. It is moderately plastic at room temperature, yet creep resistant. As a result, bicrystals of lithium fluoride were used as model specimens during this investigation.

1.1 Advantages of Lithium Fluoride

Lithium fluoride is a transparent ionic crystal and has

the rock-salt structure. The slip systems are one of the simplest to analyze. The primary slip planes are the {110}type planes and the secondary slip planes are the {001}-type. The slip directions are $\langle 1\bar{1}0 \rangle$ in both cases. There is only one <110> direction in each {110} slip plane. The slip bands due to slip in planes perpendicular to the {100} plane are known as 90° bands or orthogonal slip bands. On the other hand, the slip in planes which are at an angle of 450 to the {100} surface and intersect along <001> gives parallel slip bands are 45° bands. There can be only one kind of mobile dislocation in each active primary slip plane and hence the complication of dislocations with different Burgers vectors to be found in the same slip plane can be avoided. Initiation of secondary slip is difficult at room temperature due to the high stresses needed for moving dislocations in the secondary slip planes [1, 2]. In the rock-salt structure no two primary slip planes have the same Burgers vector, and hence cross-slip at room temperature is improbable. lithium fluoride single crystal, normally at room temperature, crack propagates along the primary cleavage planes. The primary cleavage planes of LiF are {001}-type planes and the secondary cleavage planes are {110}-type. Grain boundaries can be seen clearly by etching LiF bicrystals in very dilute solution of ferric chloride in distilled water (10⁻⁴ molal solution).

1.2 Theory of Fracture

The dominant feature of the mechanical properties of

ceramics is brittleness with virtual absence of plastic flow. This is because there is an insufficient number of independent slip systems to allow an arbitrary change of shape in one grain to be accommodated by slip in its neighbours. High stresses are thus set up near grain boundaries resulting a brittle fracture.

Brittle fracture is not possible unless the cracks which are nucleated can propagate at a high velocity (6 x 10³ cm/sec in LiF) [3] throughout the material. The elastic energy that is released by the movement of the crack is the driving force. This must be balanced by the surface energy of the new surface that is created and the kinetic energy associated with the rapid sidewise displacement of material on each side of the crack. Mott [4] has made an analysis of the velocity of a crack in an ideal elastic, isotropic medium. The crack velocity 'V' is given by

$$V = BV_O \left(1 - \frac{a_G}{a}\right) \tag{1}$$

where 'B' is a constant and 'V_O' is the velocity of sound in the material. The term 'a_G' is the length of a Griffith crack, and 'a' is the actual crack length. When 'a' is large compared with 'a_G', equation (1) approaches the limiting value 'BV_O'. The constant has been evaluated for the planestress condition and found to be B \approx 0.38 [5]. Table 1 shows that experimental values [3] for the crack velocity in brittle materials agree quite well with the theoretical prediction and that the limiting crack velocity is given by

Table 1. Velocity of propagation of brittle fracture[3]

Material	Observed velocity ft/sec	v/v _o
LiF	6,500	0.31
Steel	6,000	0.36
Fused quartz	7,200	0.42

v: velocity of crack in the material

v_o: velocity of sound in the material

$$V = 0.38 V_O = 0.38 \left(\frac{E}{\rho}\right)^{\frac{1}{2}}$$
 (2)

where E is Young's modulus and p is density of the material.

Since the bonding of atoms in crystals depends very strongly on interatomic spacings, and the spacings are disturbed near grain boundaries, it is expected that boundaries will have less strength than the crystals themselves. The effect is rather small in the case of metals so it is not difficult to obtain high-strength polycrystalline metals. The reason that the effect is small is that the cohesive energy in metals is insensitive to the exact arrangement of the atoms, much of it originating from long range interactions.

However, in ceramic crystals, atomic arrangements are far more important because of the directionality of covalent bonding, and its short range character. Therefore, it is expected that the energies of grain boundaries in ceramics will be higher relative to free surface energies than in the case of metals.

There are various ways for estimating structural weakening at grain boundaries. A few of these will be considered in turn:

(a) Examination of the bubble raft photographs of Lomer and Nye [6] suggests that about 35% of the atomic bonds are completely missing in a high angle grain boundary. Thus a strength reduction of at least this amount must occur.

However, this would be an underestimate for a

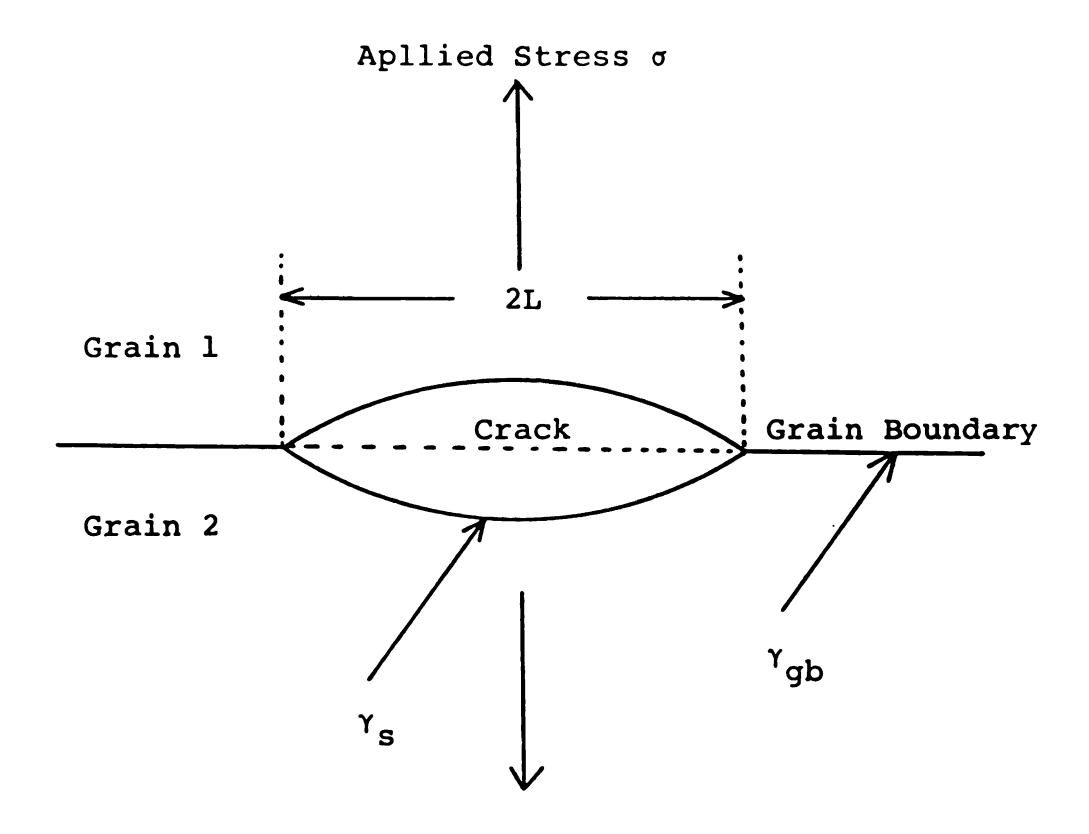


Figure 1. Schematic diagram of crack formation at a grain boundary.

covalent or ionic crystal because it does not take into account the abnormal atomic positions.

(b) A formal method consists of considering the energetics of crack formation at a boundary. The geometric situation is shown in figure 1.

The applied stress, σ , produces a strain energy density in the material of $\sigma^2/2E$ where E is the elastic modulus. Introduction of a crack of length, 2L, causes three changes. First, the strain energy in a volume of πL^2 (for unit thickness) is relaxed. This amount of energy is $-\pi\sigma^2L^2/2E$. Second, some grain boundary, of energy $-2L\gamma_{\rm gb}$, is eliminated. Third, two new free surfaces, of energy $+4L\gamma s$, are created. In order for the crack to propagate there must be a net decrease in the energy of the system. That is:

$$\frac{\pi \sigma_{fb}^2 L^2}{2E} \ge (2\gamma_s - \gamma_{gb}) 2L$$
 (3)

where σ_{fb} is the stress for fracture in the presence of the grain boundary. If no boundary is present, $\gamma_{gb} = 0$, and the stress for fracture is σ_f . Thus, the ratio of the fracture stresses in the two cases (eliminating the approximation made for the strain energy term) is:

$$\frac{\sigma_{fb}}{\sigma_{f}} = \sqrt{1 - \frac{\gamma_{gb}}{2\gamma_{g}}} \tag{4}$$

and we see that, if the grain boundary energy equals twice the free surface energy, the strength of the boundary is zero.

On the basis of the above argument, it seems quite probable that some of the grain boundaries in polycrystals of a substance would be quite weak, even in a very pure specimen. This will be equally true of any substance whose cohesion is based on nearest neighbor interactions. It is extremely difficult to obtain unambiguous information about the strength of grain boundaries because there is a strong tendency for impurities to segreate at them. The fact that polycrystalline nonmetallic substances commonly fracture intergranularly suggests boundary weakness as would be expected from the previous arguments.

2 CRYSTALLOGRAPHY

2.1 Crystal Structure of LiF

Lithium fluoride has rock-salt structure. The structure is a nearly perfect example of ionic bonding with alternate lattice points occupied by cations(Li⁺) and anions(F⁻). The unit cell is composed of eight small cubes, each of whose corners is occupied by an anion/cation. If the F ions are considered, it can be seen that they are arranged in facecentered cubic fashion, with the Li tions occupying all the octahedral interstices in this array. It can also be seen that the arrangement of F ions is the same as that of the Ti+ ions, so that the Li ions also are arranged in facecentered cubic fashion. Another way of looking at the structure is thus as two interpenetrating face-centered cubic structures, one of F ions and one of Li tions, displaced relative to each other by a distance of half the lattice parameter along one of the three major crystal directions. Thus, just as each Li⁺ ion is surrounded by six F⁻ ions at the Corners of a regular octahedron, each F ion is surrounded by six Li⁺ ions, also at the corners of a regular octahedron. Each Li⁺ ion is in six-fold coordination with oxygen atoms, each of which receives one-third of a valence share. As a consequence, all F atoms must, in turn, be in contact with six Li tions. The crystal structure of lithium fluoride is shown in figure 2.

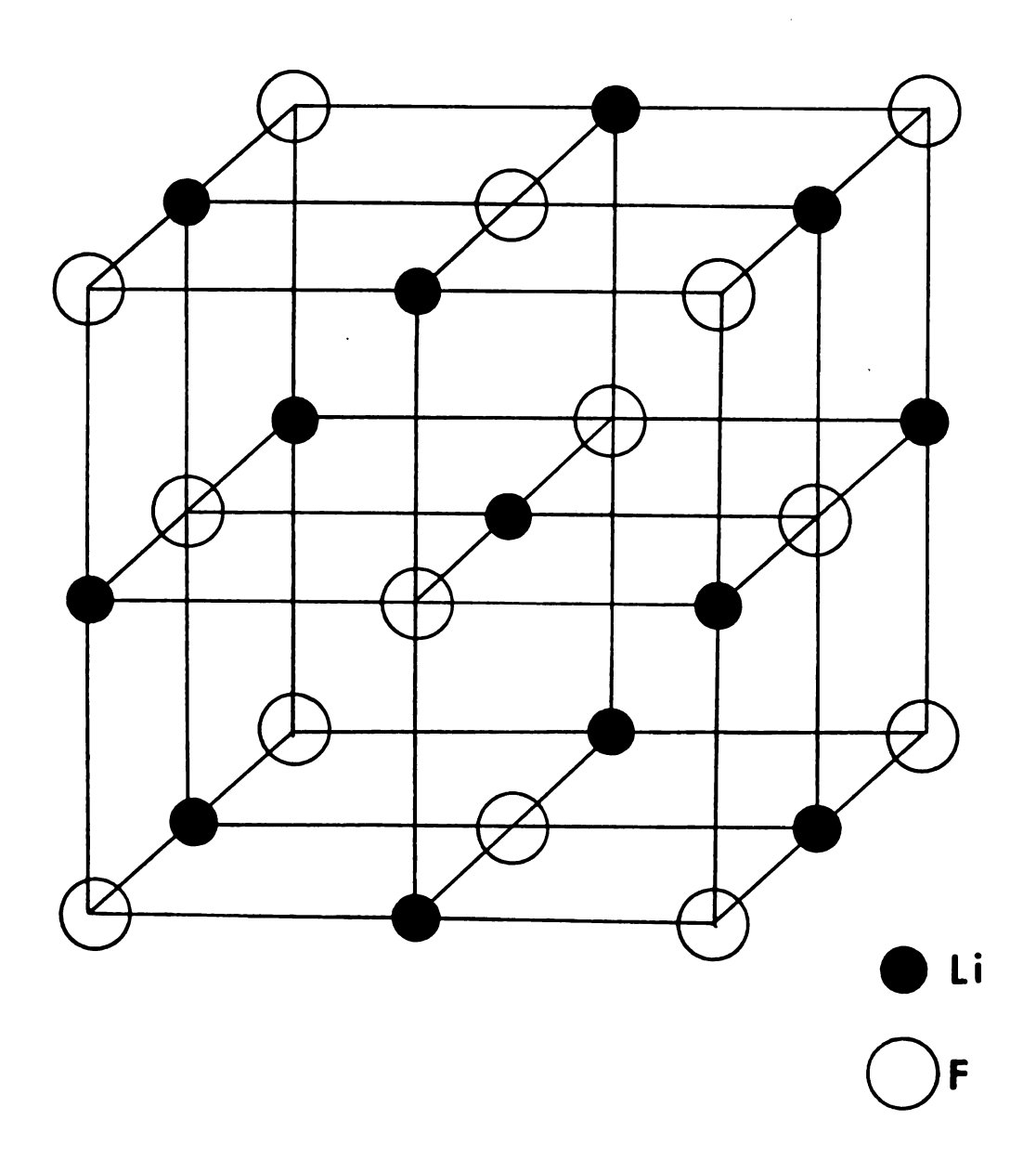


Figure 2. Crystal structure of lithium fluoride.

2.2 Deformation Behavior of LiF Single Crystal

In LiF crystals, the primary slip system is of the type {110} <110> at low temperatures. Restrictions on slip systems and slip directions result from both geometric and electrostatic considerations. Thus, in LiF crystals the direction of gliding, <110>, is the shortest translation vector of the crystal structure and requires the smallest amount of displacement across the glide plane to restore the structure. Also, translation in the <110> direction does not require any nearest neighbor ions of the same polarity to become juxtaposed during the glide process, and no large electrostatic repulsive forces develop.

There are six physically distinct slip systems: (A) (101) [101], (011) [011], (110) [110] and (B) (101) [101], (011) [011], (110) [110]. However, sets (A) and (B) each produce the same strain, because the two sets simply interchange slip plane and slip direction; therefore the two sets are interdependent. The simultaneous activity of the three slip systems produces only a rigid rotation about [111]. Thus only two of the slip systems are independent, so that LiF polycrystals can not undergo a general deformation by {110} <110> slip.

At high temperatures, the secondary slip system is $\{001\}$ <1 $\bar{1}0$ > type, and there are also six physically distinct slip systems. From the six slip systems, three independent slip systems can be chosen. Thus, $\{110\}$ <1 $\bar{1}0$ > and $\{001\}$ <1 $\bar{1}0$ > slip provide five independent slip systems.

The shortest Burgers vector for a perfect dislocation in LiF crystal structure is $\frac{a}{2} < 1\overline{10} >$. This is the operative slip direction. There is only one $< 1\overline{10} >$ slip direction in each $\{110\}$ slip plane. Therefore, there can be only one kind of mobile dislocations in each slip plane. As the primary and secondary slip planes have a common Burgers vector, this is the cross-slipping plane.

2.3 Fracture Behavior of LiF Single Crystal

2.3.1 Crack Nucleation

In semibrittle materials, the initiation of fracture results from localized plastic deformation. LiF and many ceramic materials fit into this category.

Zener proposed that localized plastic deformation could lead to initiation of a crack. A specific example of such a configuration is a pile-up of edge dislocations at an obstacle, e.g., a grain boundary.

A more general pile-up model, which does not require grain boundaries, was developed by Cottrell [7] and was found experimentally by Washburn et al. [8]. Crack is formed along the junction of two intersecting slip planes [9, 10]. If we consider an (001) cleavage plane intersected by (101) and (10 $\overline{1}$) slip planes inclined at 45° to it, they meet it along an [010] axis (figure 3(a)). A slip dislocation with Burgers vector $\frac{a}{2}[\overline{1}01]$ gliding in (101) meets along this axis a similar dislocation, with a Burgers vector $\frac{a}{2}[101]$ gliding along (10 $\overline{1}$). They coalesce to form a new dislocation, thus,

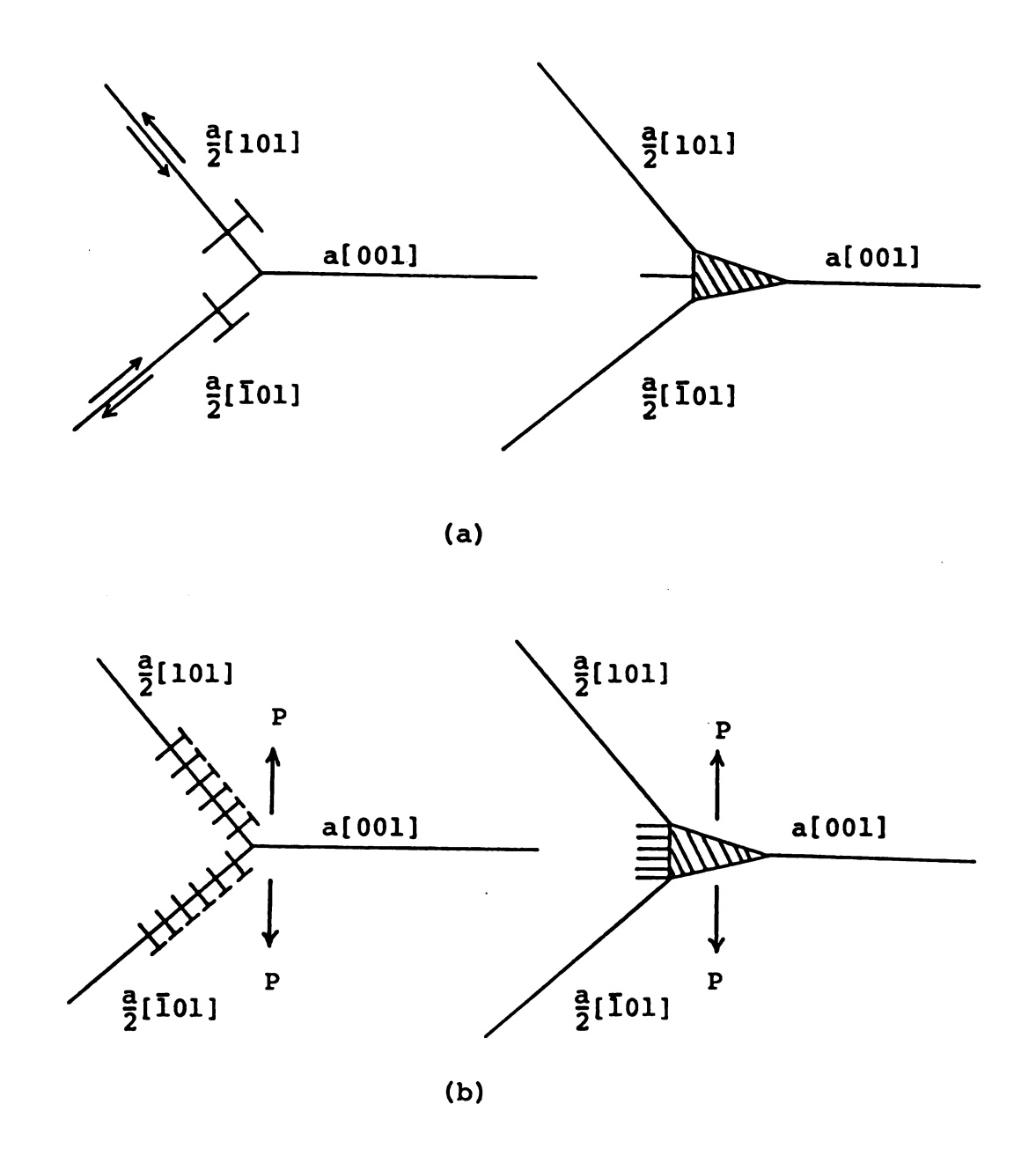


Figure 3. Crack nucleation by dislocation interaction [7]

$$\frac{a}{2}[\overline{101}] + \frac{a}{2}[101] \longrightarrow a[001]$$
 (5)

and in so doing they do not release elastic energy, and the resulting dislocation is unlikely to be stable.

The a[001] dislocation produced by the above reaction is a pure edge which lies in the (001) cleavage plane. It is thus geometrically identical with a cleavage knife, one lattice constant thick, inserted between the faces of this plane. Since this dislocation has low elastic energy and a large Burgers vector, it will act as crack nuclei, as shown in figure 3(a). This crack can grow by other slip dislocations in the (101) and (101) planes running into it, as shown in figure 3(b). The applied stress has little direct influence on the crack during the early stages of growth and acts mainly through the force it exerts on the dislocations moving into the crack. As the crack grows, however, the direct action of the stress on it becomes more important and eventually predominates as the crack becomes longer than the slip bands from which it originated.

Also, Keh et al. [1] showed that cracks can form as a Consequence of nonorthogonal {110} slip bands. The tendency to form cracks at glide band intersections is greatest at Very low homologous temperatures (about 77° K for LiF), for wide slip bands, and for large slip band spacings. When slip bands are very finely distributed, crack formation at slip band intersections is suppressed.

2.3.2 Crack Growth and Propagation

In order to fully understand the mechanism of crack nucleation in crystals, it is necessary to have a good understanding of the processes that occur during crack propagation.

By the Griffith theory of crack propagation, the condition for crack propagation is that:

$$\gamma_{f} < \frac{A\sigma^{2}L}{E} \tag{6}$$

where γ_f = fracture surface energy

 $A = constant(\frac{\pi}{2})$

 σ = tensile stress

L = crack length

E = Young's modulus.

The value of γ_f depends on the speed of a crack, the structure of the crystal, the temperature, and its cohesive strength. The maximum speed of a crack in a crystal is determined by the velocity of sound waves in it. In LiF crystals, the maximum velocity is 2 x 10⁵ cm/sec along {100} planes.

When a crack moves slowly through an ionic crystal, the motion is not elastic because dislocations are nucleated near the tip of the crack. In LiF crystals, the critical velocity below which dislocation nucleation occurs is about 6×10^3 cm/sec at room temperature. At velocities below 23×10^3 cm/sec crack in LiF crystals propagate in an

unstable fashion; that is, their velocities oscillate between high and low values [3]. Each time they slow down, they form groups of dislocations. If sufficient time is available after dislocations have been nucleated by a moving crack, they can causes appreciable amounts of plastic flow, thereby causing a large amount of energy absorption from the moving crack.

Some crystal defects, such as lattice vacancies and impurity atoms have little effect on the ease of crack motion. Defects that have a large effect on crack propagation are screw dislocations [12]. A screw dislocation converts the crystallographic planes that lie perpendicular to it into a helical ramp. Therefore, when a crack runs along one of the planes and intersects the screw dislocation, it splits into two parts. The two parts move along planes that are separated from each other by a distance equal to the component of the deslocation Burgers vector that lies perpendicular to the planes. Eventually the two halves of the crack join together along a step. Such steps can easily be seen on the surfaces of cleaved crystals and they corelate closely with etch pits at screw dislocations in the crystals.

LiF crystals prefer to cleave along {001} planes. Thus these planes have the minimum surface energy. Secondary cleavages are along {110} under certain conditions. The surface energy of {001} plane is 340 ergs/cm² and that of {110} plane is 850 ergs/cm² at -196°C [13].

In a perfect crystal, a fast-moving crack is only

impeded in its motion by the energy required to make the new surfaces of the crack, and by the inertial mass of the crystal. In imperfect crystals, other effects act to impede the motion of cracks. The most important of these effects is the plastic deformation that can occur at the tip of a slowly moving crack. In a crystal that contains screw dislocations, a crack front must split into two parts each time it intersects a screw dislocations, and this provides another impediment to the motion of the crack. Also, edge dislocations can have an effect because the cohesion of a crystal is reduced at their centers.

Cracks can move as fast as 2 x 10⁵ cm/sec along {100} planes in LiF crystals. This maximum, or terminal, velocity is limited by the inertia of the crystal as it opens up to form the crack. At crack velocities near the terminal value, there is no time for dislocation nucleation; but at a much lower velocity (\$6 x 10³ cm/sec) dislocation loops begin to form in front of a crack tip. This is only an approximate value of the critical velocity because it varies with the flow stress of each particular crystal. The higher the flow stress, the lower the critical nucleation velocity.

If the velocity of a crack is allowed to drop below the critical value, the dislocations that are nucleated move increasingly large distances during crack propagation, and cause increasing amounts of plastic flow. At velocities less than about 50% of the critical velocity enough plastic flow occurs to make crack propagation unstable [3].

The dislocations that form in front of cracks are often small complete loops and they form at places where no dislocations existed previously. Thus a crystal need not contain dislocations initially in order for plastic flow to occur in it and impede crack propagation. By blunting the sharp edge of a crack, plastic flow reduces its stress-concentrating effect and therby makes it difficult for the crack to move. However, according to impact tests on notched specimens by Johnston et al., this effect is not large in LiF until temperatures above about 400°C are reached.

The screw dislocations may be present in several forms: as twist-type sub- boundaries: within glide-bands that result from plastic deformation; or as parts of the small dislocation loops that nucleate ahead of moving cracks. The fracture energy of a surface that is roughened by the presence of many cleavage steps is higher than the energy of a smooth surface.

3 GRAIN BOUNDARY

3.1 Role of Grain Boundry in Deformation

An extension of available knowledge obtained from the deformation of single crystals to polycrystals is very difficult owing to the imposition of additional constraints by the grain boundaries. Extensive investigations have been carried out with bicrystals in order to understand the constraints imposed by the grain boundary on the deformation [14-21]. It was observed that slip lines in many cases are continuous across the boundary. Furthermore, additional slip systems were found of be activated in both grains. The continuity of slip across the boundary implies that glide dislocations pass through the boundary and that the boundary itself undergoes deformation because of this passage [22]. The ease with which the boundary undergoes deformation should control the ease with which slip can propagate from one grain to the other.

For a complete mathematical description of a boundary separating two crystals, five parameters are necessary since such a boundary has five degrees of freedom. For a consideration of the shear of the boundary by the passage of dislocations across it, it is advantageous to prescribe the above five parameters in terms of the slip systems directly, instead of in terms of Eulerian angles. Both descriptions, however, are essentially the same. Figure 4(a) shows how the grain boundary is specified with respect to the two slip

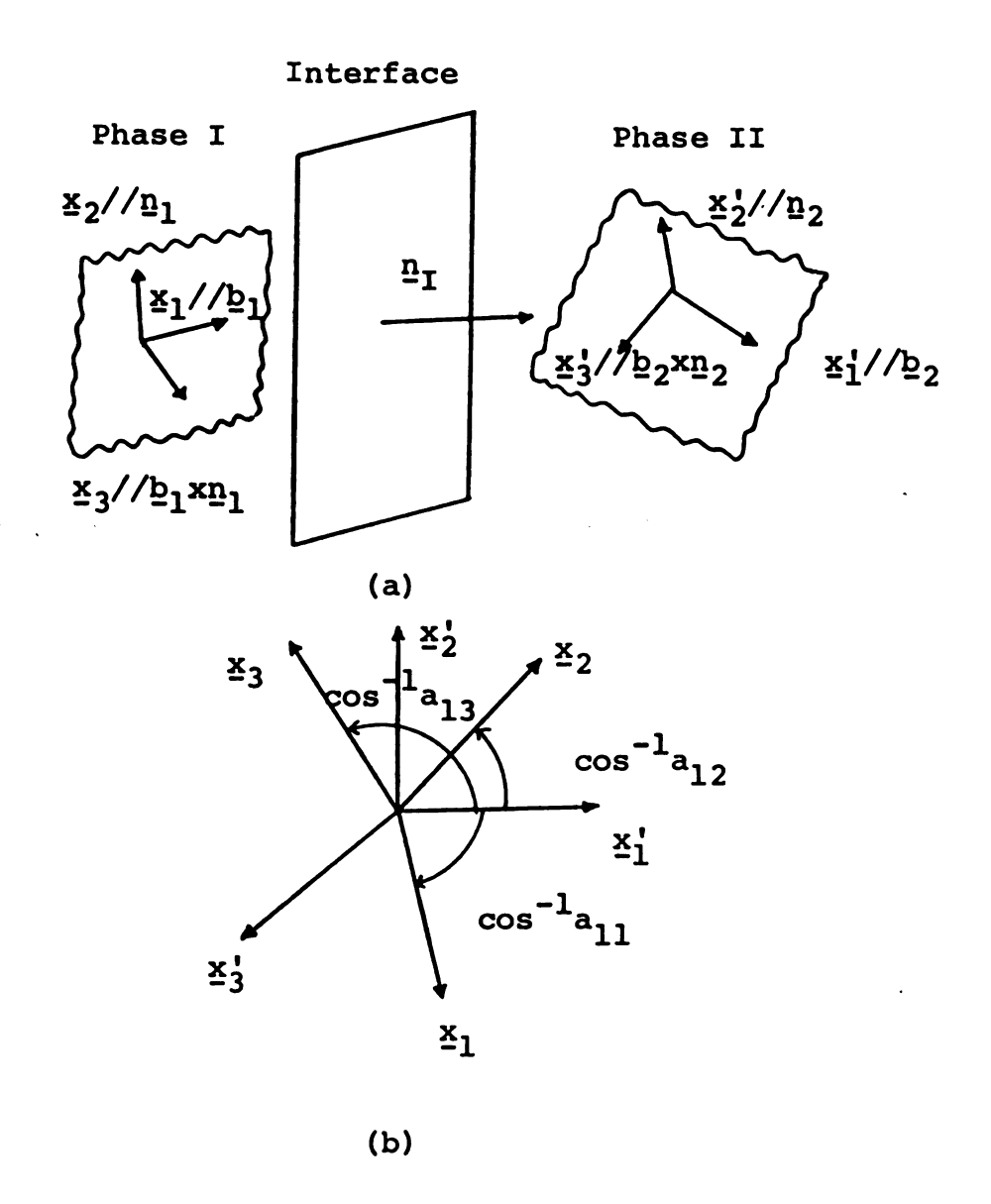


Figure 4. (a) Coordinate axes in two adjacent phases

(b) Relationship between the two systems

of coordinates.

systems in adjacent grains.

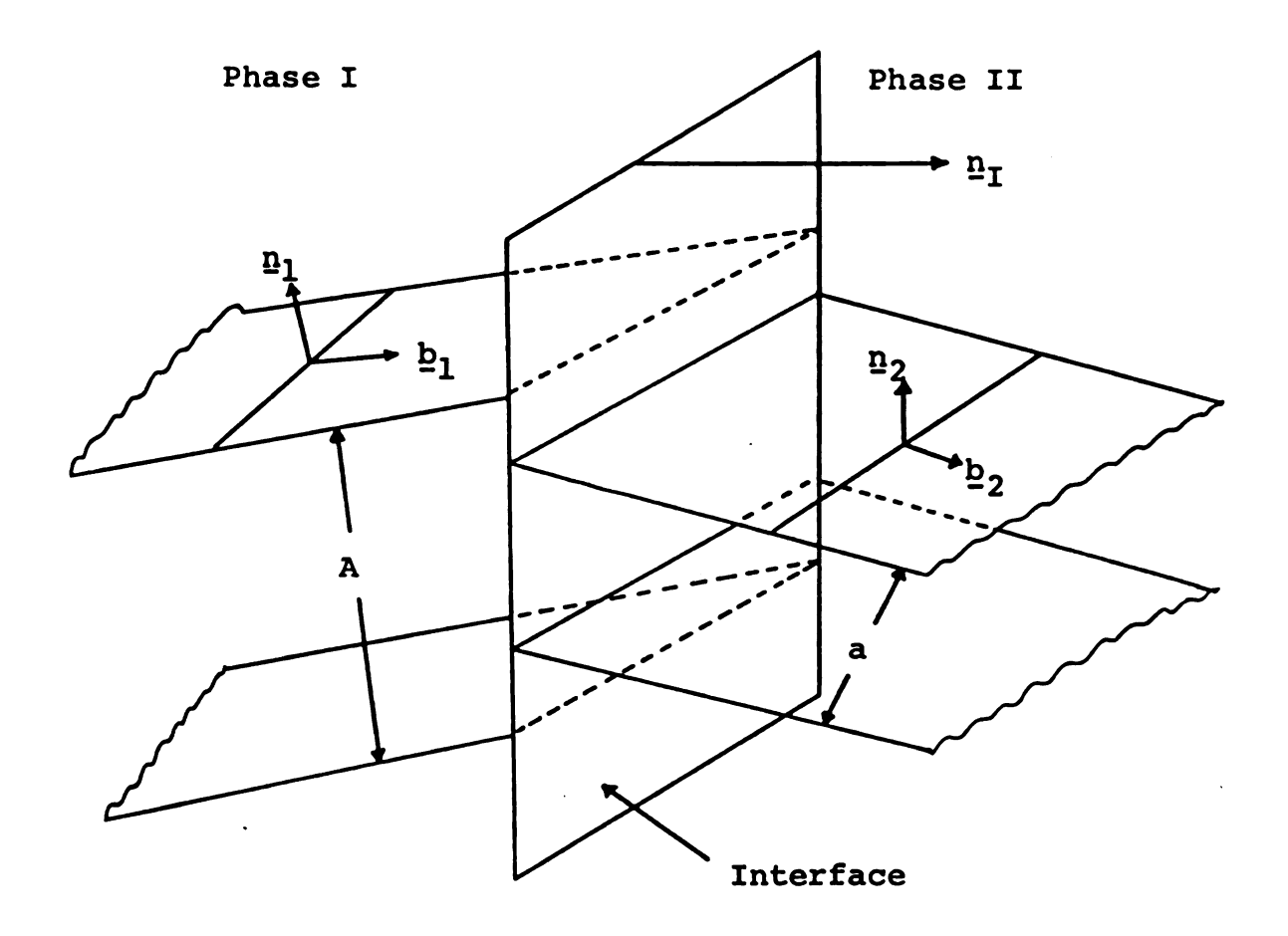
The reference coordinates, \underline{x}_1 , \underline{x}_2 , \underline{x}_3 are chosen to be parallel to \underline{b}_1 , \underline{n}_1 and \underline{b}_1 x \underline{n}_1 respectively, where \underline{b}_1 is the Burgers vector normal to the slip plane in crystal I. The coordinates \underline{x}_1' , \underline{x}_2' , \underline{x}_3' correspond to \underline{b}_2 , \underline{n}_2 and \underline{b}_2 x \underline{n}_2 respectively, where \underline{b}_2 and \underline{n}_2 specify the slip system in crystal II. The outward normal to the boundary before deformation is denoted by \underline{n}_1 . The relation between the two systems of coordinates is shown in figure 4(b).

Figure 5 schematically illustrates the passage of a dislocation from crystal I to crystal II. In general, the magnitude of the Burgers vector and the interplanar distances 'A' and 'a' need not be the same as indicated in figure 5. In such cases, the continuity of slip planes across the interface is established by the presence of interface dislocations. Due to the relative rotation of the two slip systems as well as to the difference in the magnitude of the slip vectors, a disturbance is left at the boundary when a dislocation passes from one crystal into the other. Such a disturbance is characterized by an effective Burgers vector given by

$$\underline{b}_{I} = (\underline{b}_{1} - \underline{a}\underline{b}_{2}) \tag{7}$$

Here subscripts I refers to the grain boundary plane.

As a result of the shear, the boundary itself undergoes shape and orientation changes which can be determined from



A: Magnitude of the Burgers vector

a: Interplanar distance

Figure 5. Passage of a dislocation from one crystal into the other.

the geometrical properties of the dislocation responsible for the shear. When a dislocation with Burgers vector \underline{b}_1 cuts through the boundary, it leaves a ledge in the boundary, the component of its height normal to the boundary, h_1 , is given by

$$h_1 = \frac{(b_1 \cdot n_1) + (b_2 \cdot n_1)}{2}$$
 (8)

In cases where the ledges are formed in the boundary, the ledges and their associated dislocation are to be considered as one entity since one cannot be separated from the other. Whenever the ledge moves, either by glide or by climb, the boundary undergoes migration [22]. Boundary sliding could also occur along with migration if the dislocations associated with the ledge have Bugrers vector components parallel to the boundary. Many experimental observations show that grain boundary sliding almost always occurs along with grain boundary migration [23].

The displacement of the boundary as a result of its migration owing to the motion of the ledge is given by the component of the height of the ledge normal to the boundary, h₁ (Equation 8). On the other hand, the magnitude of sliding is given by the magnitude of the component of the Burgers vector of the interface dislocation parallel to the boundary, i.e., by

$$\underline{\mathbf{h}}_2 = \underline{\mathbf{b}}_{\mathbf{I}} - (\underline{\mathbf{b}}_{\mathbf{I}} \cdot \underline{\mathbf{n}}_{\mathbf{I}}) \underline{\mathbf{n}}_{\mathbf{I}} \tag{9}$$

3.2 Role of Grain Boundary in Fracture

Accommodation problems for LiF single crystals become more severe in LiF polycrystals. Here the barriers to slip are grain boundaries and not other slip bands. The highly localized shear strain associated with slip in one grain of a LiF bicrystal at room temperature cannot be absorbed at all in the grain across the boundary. There is absolutely no source of accommodation other than elastic distortion of the adjacent grain. The inevitable result is the generation of a crack whenever a slip band intercepts the grain boundary.

For unrestricted plastic deformation each of the grains should be capable of undergoing a perfectly general change in shape. According to the Von Mises criterion this is only possible when the crystalline slip parameters give rise to five independent slip systems. If there are less than five, the plastic strain due to one grain cannot be completely accommodated by its neighbors and high internal stresses develop across grain-boundary interfaces.

Another important example of crack initiation resulting from plastic flow is that due to the interaction of glide bands with grain boundaries. Westwood [24] first observed the formation of grain boundary cracks in MgO bicrystals at room temperature. Such cracks forms as a result of stress concentrations of two glide bands, one on each side of the boundary, superimpose. Johnston et al. [25] demonstrated that the stress concentration associated with a single glide

band is also capable of nucleating a crack at the boundary of MgO bicrystal at room temperature. The orientation of the initial crack relative to the nucleating glide band varies widely. It depends upon the state of the applied stress and the degree of misorientation across the boundary. The crack, which starts at the tip of the nucleating glide band, may spread along the boundary, or it may propagate into either grain along a (100) or (110) plane. If there is a tensile component of stress across the boundary, the intergranular path is favored for both high angle and medium misorientation angles (tilts and twists 10°). Regardless of the nature of the initial crack, i.e., whether it propagates through the grain or along the boundary, the crack lies on the obtuse side of the band in tension. For simple tilt boundaries, the stress concentration is generally relieved by the nucleation of glide bands in the neighboring grain rather than by fracture.

4 EXPERIMENTAL PROCEDURE

4.1 Bicrystal Growth

Some of the crystals grown by Bridgman method had approximately <100> as the direction of growth, and these were cleaved and used as seeds to grow lithium fluoride single crystals. Lithium fluoride powder, obtained from KAWECKI Chemical Company, was used and had the chemical composition given in the table 2.

Lithium fluoride single crystals were grown by the Czochralski method (figure 6) under the conditions and improvisations described below for achieving faster growth rates with relatively perfect crystallographic orientations. The high density-graphite crucible, holding the melt, and the seed were rotated in opposite directions at the rate of approximately one to two revolutions per minute to obtain a homogeneous melt and a planar solid-liquid interface. furnace was water-cooled. The rod holding the seed was also water-cooled to maintain a necessary longitudinal temperature gradient. The heating element was made of graphite. Two chromel-alumel thermocouples were placed at diametrically opposite points, and a potential-divider circuit was used to find the average thermo-emf. Argon gas was used to provide an inert furnace atmosphere. A small positive pressure of argon atmosphere was maintained in the furnace to obtain an inert atmosphere. The crystals were

Table 2. Chemical composition of LiF powder

Lif	99.200 %
н ₂ 0	0.700 %
so ₄	0.050 %
Acidity as HF	< 0.040 %
Fe ₂ O ₃	< 0.020 %
Na	< 0.005 %

(Weight percent)

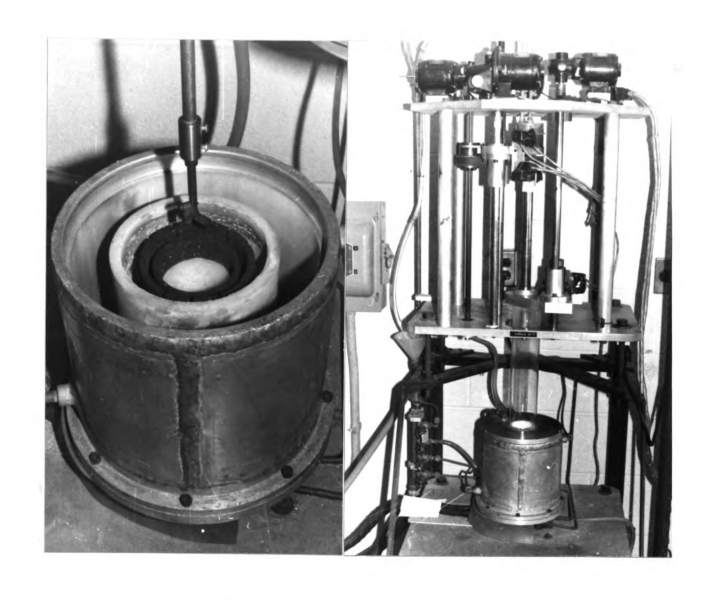


Figure 6. Czochralski furnace for growing LiF bicrystals.

grown at the rate of &" to &" per hour.

To avoid sub-boundaries propagating from the seed during the growth process, off-centering and necking nethods were employed. The growth prefers to follow the common axis of rotation [26], thereby introducing an initial curved growth immediately next to the seed if the seed is made in contact with the melt at a point away from the axis of rotation. This is called the off-centering. In the necking technique, the crystals were at first pulled out much faster than the normal growth rate. This made the crystals grow as thin as needles. After some time, the growth rate was decreased and the temperature of the melt reduced in order to obtain crystals of the required size. The formation of a neck between the seed and the growing crystal prevented most of the sub-boundaries in the seed from propagation into the grown crystals. These single crystals having relatively perfect crystallographic orientation were cleaved and used as seeds to grow lithium fluoride bicrystals.

Lithium fluoride bicrystals were grown by the Czochralski method from lithium fluoride powder using two LiF single crystal seeds. To grow bicrystal, two LiF single crystal seeds oriented differently were used together as seeds. The procedures of growing the bicrystals by the Czochralski method were the same as that mentioned above. The two seeds were held by two seed rods fixed at 45° to each other. In each seed rod the seed could be set at any

rotation since these were held by set screws. For the pregent experiments the bicrystals were grown with a constant tilt angle of 45° and at various twist angles.

4.2 Specimen Preparation

The LiF bicrystals were cut with a low speed saw having thin diamond blade. To cut safely without damaging the grain boundary, the cutting speed was kept extremely slow. The thickness (2.5 mm) of the specimen was the same in all specimens. The bicrystal was cut so that the surface of the crystal A is (001) plane and that of the crystal B is (011) plane. So far as possible, the specimens were also cut so that the grain boundary lay transverse across the mid-section of the specimen as indicated in figure 7. specimens were indexed by X-ray back-reflection Laue Triangular shaped specimens were cut with a crystal saw and were etched with a very dilute solution of ferric chloride in distilled water (10⁻⁴ molal solution). To reduce the weakening effect of etching on grain boundary, specimens were etched very lightly. After etching, grain boundaries were relatively clear enough to be seen with the optical microscope.

Freature surfaces of selected specimens were etched to investigate cleavage steps and dislocation etch pits.

dilute ferric chloride solution was used also as etchant.

Etched specimens were washed in distilled water and rinsed in ethyl alcohol and ether and dried.

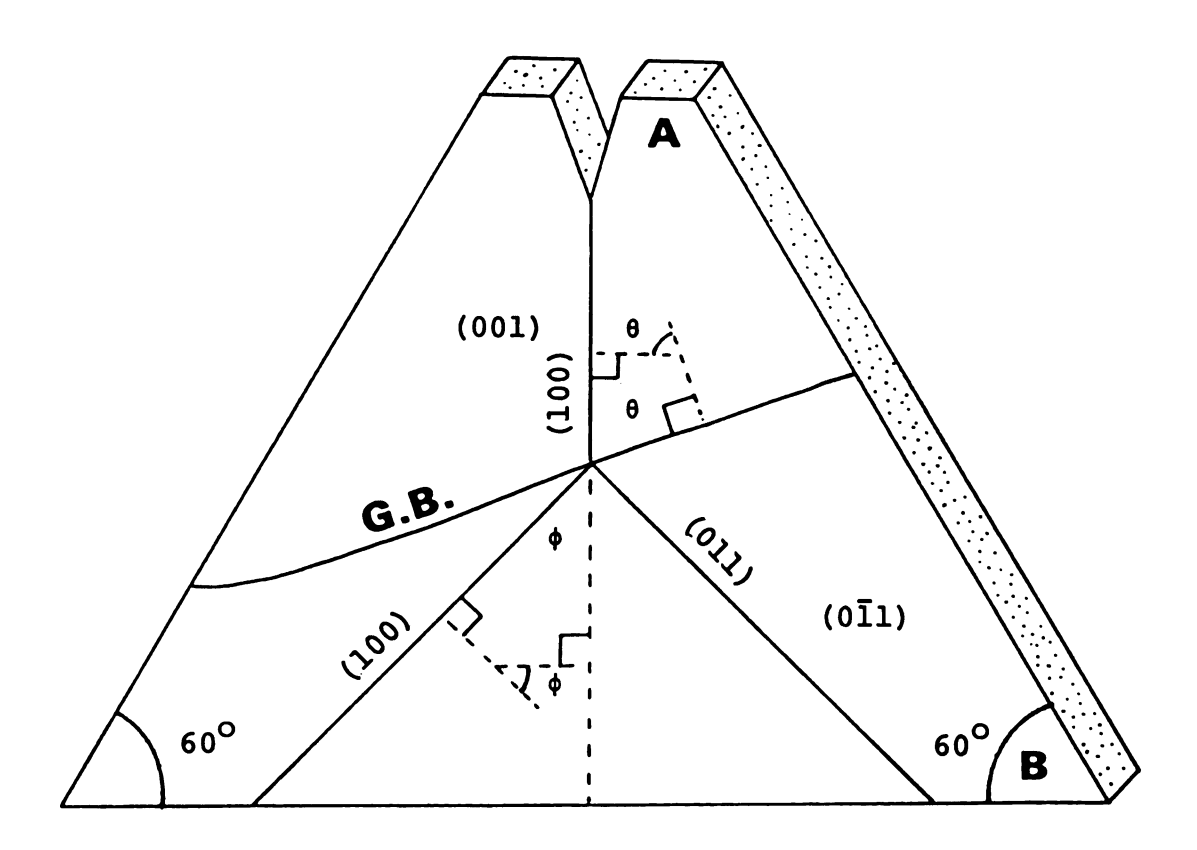


Figure 7. Specimen geometry.

Selected specimens were coated with a thin (about 100 Å) layer of gold in a sputtering equipment. This was done to eliminate charging on the surfaces of the specimens during scanning electron microscope studies since the specimens were electical nonconductors.

4.3 Test Fixture

The test fixture used for measuring the fracture load is similar principle to the one used by Gilman [27] for measuring the surface energies of crystals. A schematic drawing and picture are shown in figure 8. It consists of a screw-driven hardened steel wedge for starting crack. The wedge was ground to a 30° chisel wedge with convex curvature so it made initial contact with a crystal at only one point. The load was applied by slowly pushing the wedge into the crack by turning the drive screw with hand. measure this load a load cell was used. Four micro-strain gages were nounted on a aluminum block having dimensions of 9 mm wide, 1.5 mm thick and 22 mm long. To make it sinsitive enough to very small load, thin aluminum block was used. These micro-strain gages were connected to an amplifier which converts the strain(resistance) to that of voltage. The change of voltage was read by the digital multimeter, and the load cell and digital multimeter were calibrated by the INSTRON universal testing machine in the test set-up. 23.4 mV corresponded to one kg loading.

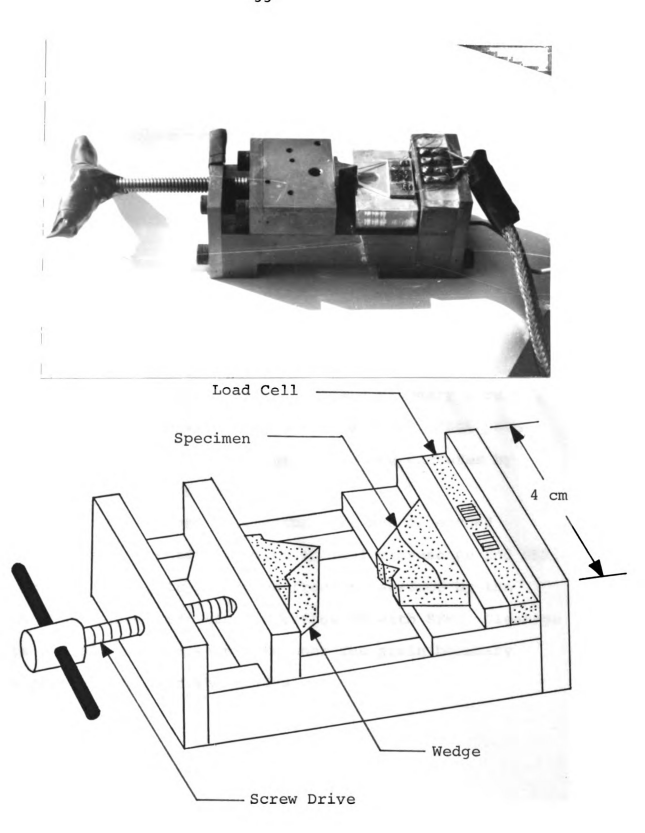


Figure 8. Test fixture for fracture load measurement.

4.4 Test Procedure

Forty-one specimens were prepared from twelve LiF bicrystals having different relative crystallographic and grain boundary orientations.

The etched triangular specimens were bisected by crack initiated at notch. The fracture loads applied by screwdriven wedge were measured by a load cell and from the geometry of the wedge, tensile components of fracture loads were calculated.

The crack paths were observed by an optical microscope having long focal length. The magnification range used was 30-100X. The crack paths near the grain boundary were photographed for the analysis. The angles of crack paths and grain boundaries were measured from the pictures by accurately graduated protractor.

The cleavage steps of fracture surface of etched specimens were investigated with optical microscope and SEM. Dislocation etch pits formed on fracture surface by the crack propagation were also investigated with SEM. Cleavage steps and dislocation etch pits near the grain boundary were photographed for the analysis.

5 RESULTS

5.1 Measurement of Misorientation Angles

Using optical micrographs of the fractured specimens, crack paths were analyzed. Measurement of the angles between crack paths and grain boundaries makes it possible to find out the misorientation angles.

The measured values of misorientation angles in all the forty-one specimens tested are included in table 3. Specimens were cut from twelve different LiF bicrystals grown with different twist angles ϕ . Crystal orientations were controlled by twist angles ϕ . Thus, all specimens from one bicrystal have the same ϕ value.

Cracks initiated from notch grew along the (100) primary cleavage plane in crystal A and propagated along the grain boundary or propagated across the grain boundary into the crystal B. The crack paths were dictated according to the relative crystallographic and grain boundary orientations. The misorientation angles of some specimens (figure 9, 10) are almost zero, so that the crack paths looks like a straight line. When the misorientation angles (ϕ) were small, transcrystalline fractures occured as shown in figure 9 to 13. But, when the misorientation angles were larger than the critical angles, the crack propagations were intercrystalline as shown in figure 14 to 15. When ϕ values are similar to critical angle (ϕ = 54.5°),

primary and secondary cleavage occured simultaneously as shown in figure 16.

5.2 Measurement of Fracture Loads

By using load cell and testing fixture shown in figure 8, fracture loads were also measured. The measured values of fracture loads are also listed in table 3.

Voltage change of 23.4 mV was found to be equivalent to l kg load. Thus the compressive component of fracture load, P_{C} , is obtained by equation 10.

$$P_{C} = \frac{\text{voltage change in mV}}{23.4}$$
 (kg) . (10)

The apex angle of the wedge is 30° , therefore, tensile component of fracture load, P_{+} , is obtained by equation 11.

$$P_{t} = \frac{P_{c}}{\tan 15^{\circ}}$$
 (kg) . (11)

5.3 Fracture Surface Studies

By investigating fracture surfaces of specimens with optical microscope, cleavage steps were found in crystal B. These cleavage steps are formed when a crack intersected the twist boundary. Some typical pictures of the cleavage steps are shown in figure 17 to 19. The density and height of these cleavage steps seem to depend on the twist angle of

the boundary. As the twist angle increases, number of cleavage steps to the step height increase as can be seen in figures 17 and 19.

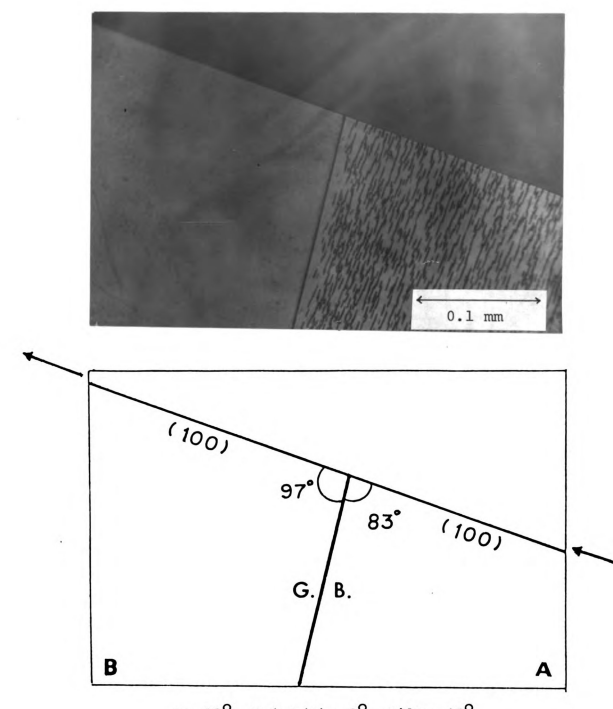
By etching technique, dislocation etch pits were investigated with optical microscope and scanning electron microscope. Figures 21 to 24 show the typical distribution of dislocation etch pit in the region near the boundary. Slip lines are also shown in figure 20.

For the preparation of SEM specimen, gold sputtering was done on the surface of etched specimens. In general, the distribution of etch pits is uniform as shown in figures 21 to 24.

Table 3. Fracture mode and fracture load for various $\boldsymbol{\theta}$ and $\boldsymbol{\phi}$

	1		 		Y	
specimen number	θ ^O	φ°	fracture load mV P _t (kg)		fracture mode	
1	83	0	160	25.52	transcrystalline(1)	
2	89.5	1	120	19.14	transcrystalline(1)	
3	87	1	290	46.25	transcrystalline(1)	
4	55	2	60	9.57	transcrystalline(1)	
5	84	3			transcrystalline(1)	
6	84	3	100	15.95	transcrystalline(1)	
7	89.5	4	140	22.33	transcrystalline(1)	
8	70	5	140	22.33	transcrystalline(1)	
9	31	5	70	11.16	transcrystalline(1)	
10	84	7	100	15.95	transcrystalline(1)	
11	85	7	140	22.33	transcrystalline(1)	
12	86	7	140	22.33	transcrystalline(1)	
13	88.5	11.5	120	19.14	transcrystalline(1)	
14	83	33	210	33.49	transcrystalline(1)	
15	89	33	190	30.30	transcrystalline(1)	
16	70	33	20	3.19	transcrystalline(1)	
17	71	33	30	4.78	transcrystalline(1)	
18	77	33			transcrystalline(1)	
19	36	42	100	15.95	transcrystalline(1)	
20	90	45	10	1.59	transcrystalline(1)	
21	88	45	300	47.85	transcrystalline(1)	
22	89	45			transcrystalline(l)	
23	42	52	50	7.97	intercrystalline	

						
specimen	_θ ο	φ ^O	fracture load mV P ₊ (kg)		fracture mode	
number			MA	t (kg)		
24	58	52	510	81.34	branching	
25	59	52			transcrystalline(1)	
26	67	54	290	46.25	branching	
27	78	58	300	47.85	branching	
28	60	78	220	35.09	transcrystalline(l)	
29	12	80	130	20.73	intercrystalline	
30	20	80	190	30.30	intercrystalline	
31	30	80	310	49.44	intercrystalline	
32	35	80	550	87.72	intercrystalline	
33	13	82	180	28.71	intercrystalline	
34	86	82			transcrystalline(2)	
35	73	82			transcrystalline(2)	
36	14	86	60	9.57	intercrystalline	
37	22	86	220	35.09	intercrystalline	
38	24	87	270	43.06	intercrystalline	
39	18.5	87	140	22.33	intercrystalline	
40	34	87	250	39.87	intercrystalline	
41	15	87		,	intercrystalline	



 θ : 83°, Twist(ϕ): 0°, Tilt: 45° Magnification: 80%, Specimen number: 1

Figure 9. Transcrystalline crack propagation along the primary cleavage plane.

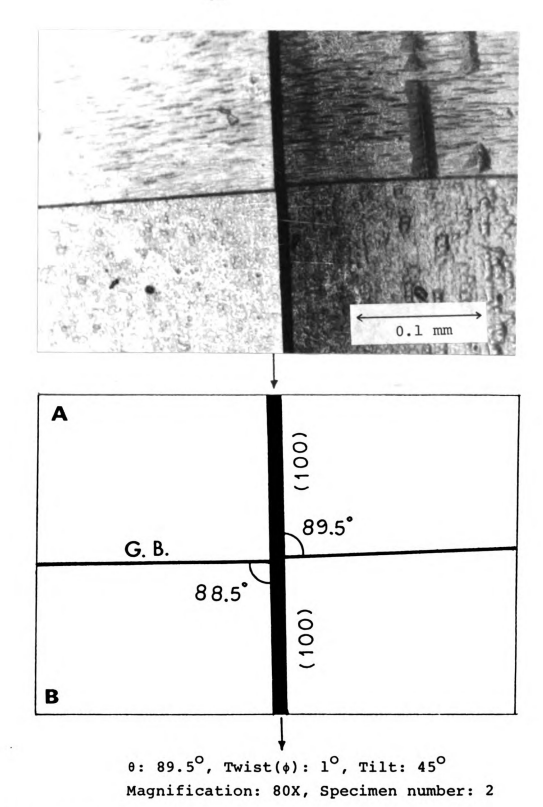
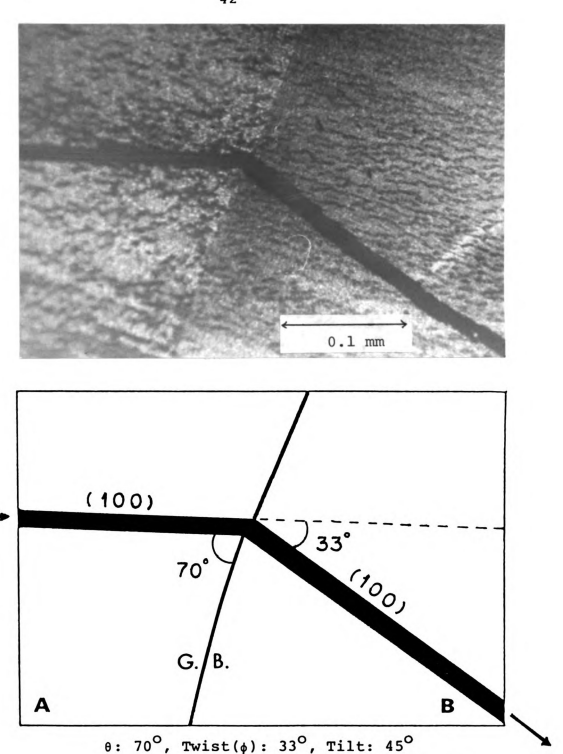


Figure 10. Transcrystalline crack propagation along the primary cleavage plane.



Magnification: 80X, Specimen number: 16

Figure 11. Transcrystalline crack propagation along the primary cleavage plane.

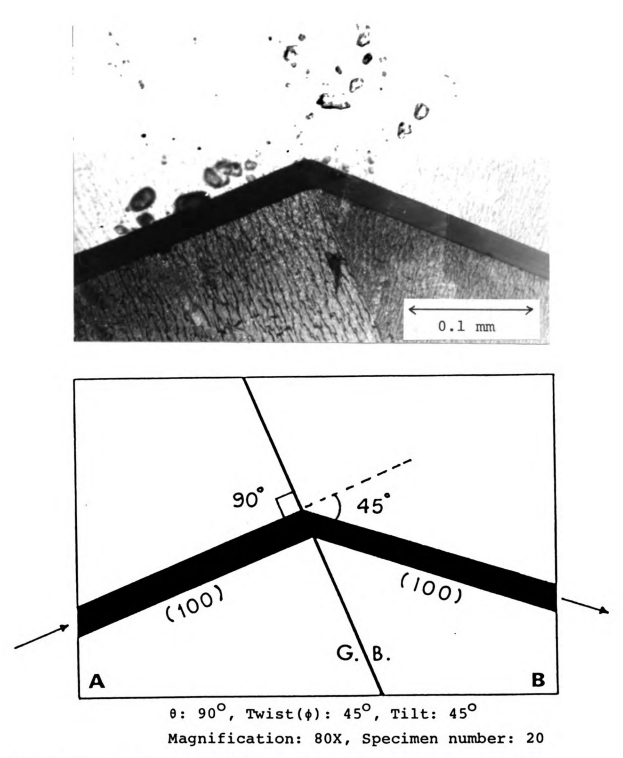
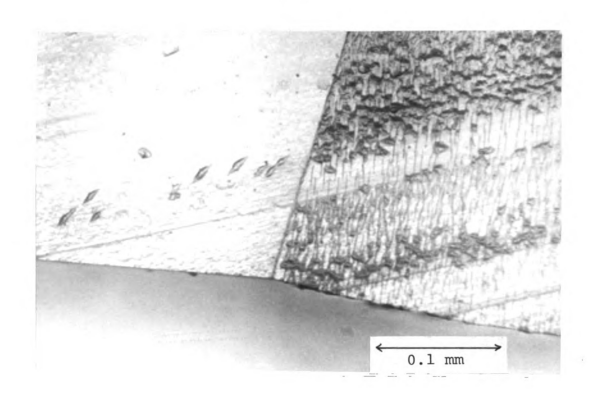
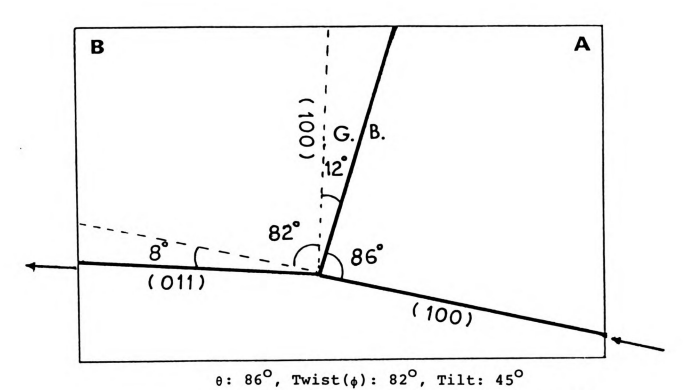


Figure 12. Transcrystalline crack propagation along the primary cleavage plane.

	· · · · · · · · · · · · · · · · · · ·		
			1
			•





Magnification: 80X, Specimen number: 34

Figure 13. Transcrystalline crack propagation along the secondary cleavage plane.

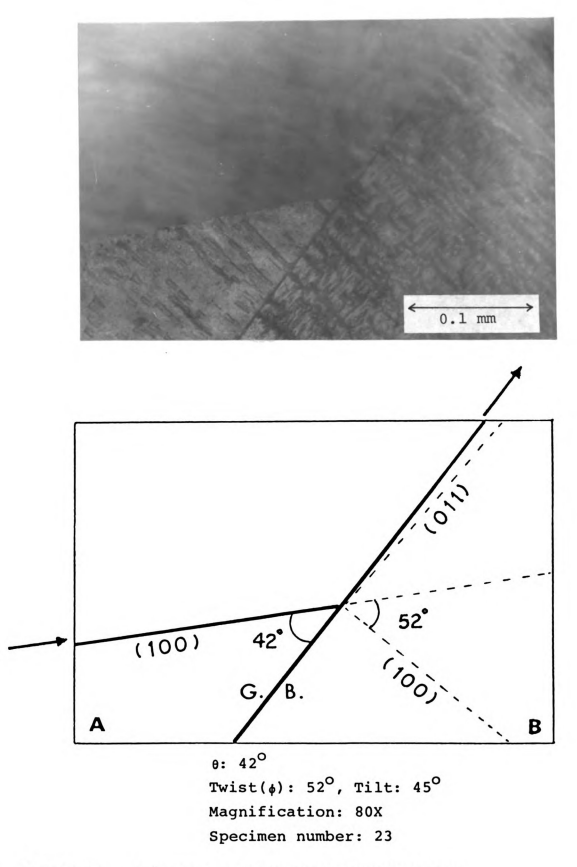


Figure 14. Intercrystalline crack propagation.

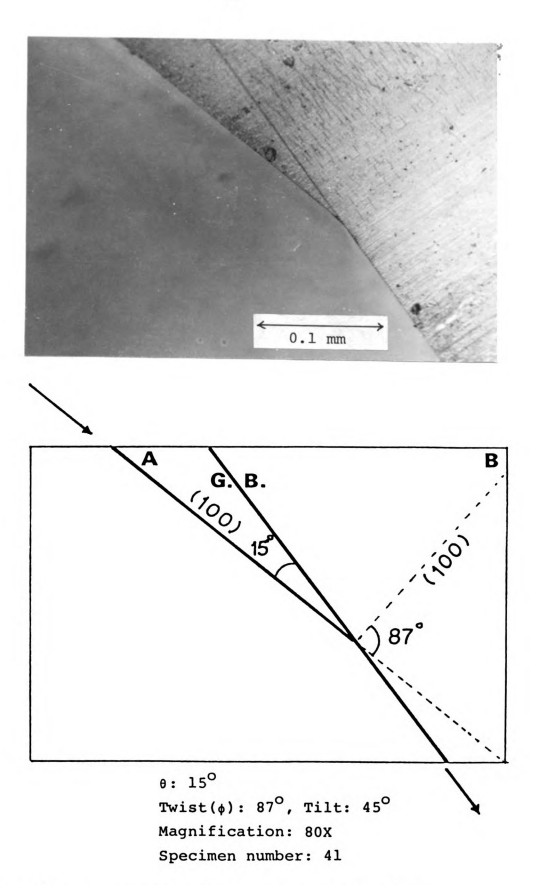
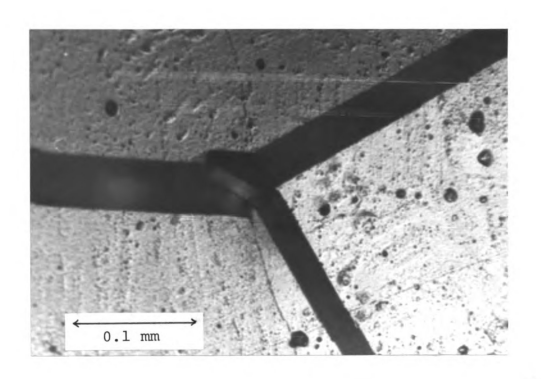


Figure 15. Intercrystalline crack propagation.

		1
	·	



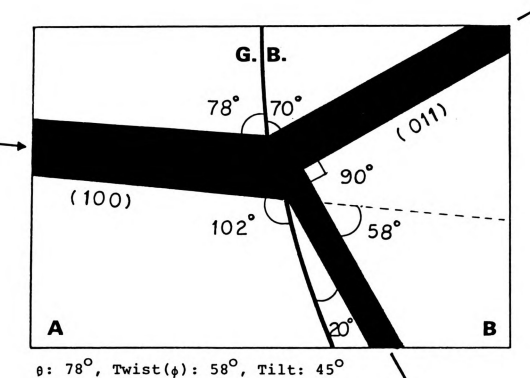


Figure 16. Crack path branching.

(primary and secondary cleavage)

Magnification: 80X, Specimen number: 27



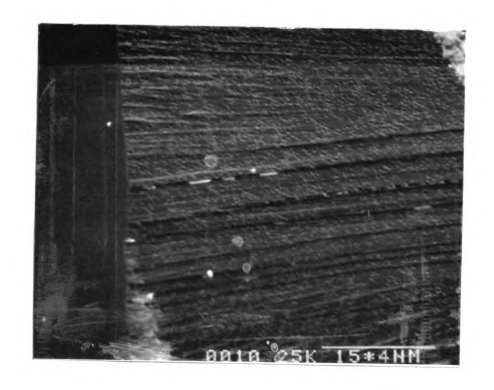
0: 88.5°
Twist(\$\phi\$): 11.5°
Tilt: 45°
Magnification: 200X
Specimen number: 13

Figure 17. Cleavage steps formed by the crack passage through grain boundary.



e: 36^o
Twist(\$\phi\$): 42^o
Tilt: 45^o
Magnification: 80X
Specimen number: 19

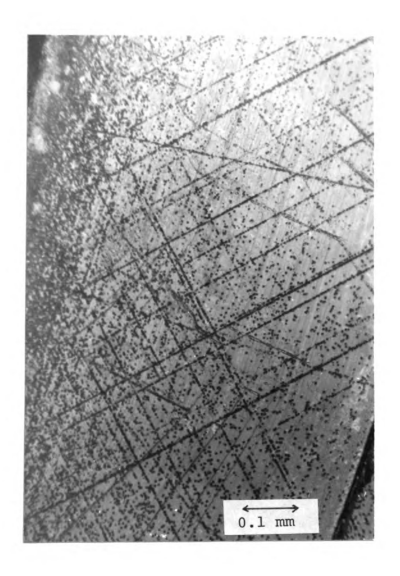
Figure 18. Cleavage steps formed by the crack passage through grain boundary.



6: 12⁰
Twist(\$): 80⁰
Tilt: 45⁰
Mabnification: 200X(SEM)
Specimen number: 29

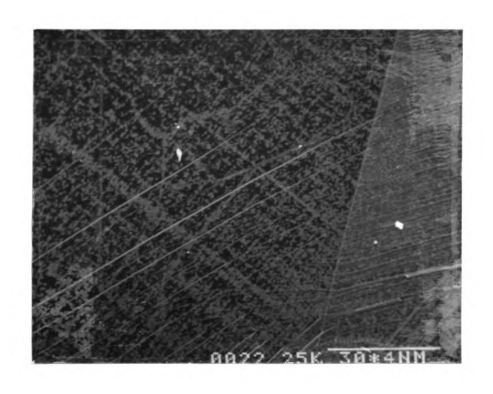
Figure 19. Cleavage steps formed by the crack passage through grain boundary.

51



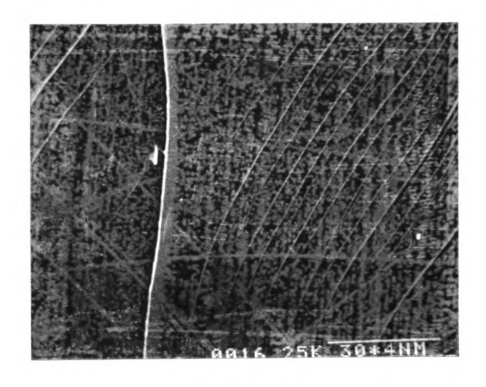
6: 89.5°
Twist(\$\phi\$): 4°
Tilt: 45°
Magnification: 200X
Specimen number: 7

Figure 20. Slip lines formed by crack propagation.



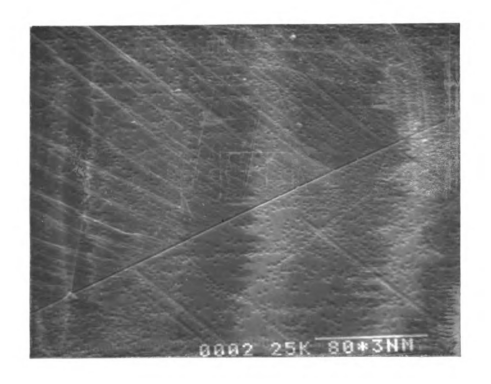
0: 89.5°
Twist(\$): 4°
Tilt: 45°
Magnification: 100X(SEM)
Specimen number: 7

Figure 21. Uniform distribution of dislocation $\qquad \qquad \text{etch pits.}$



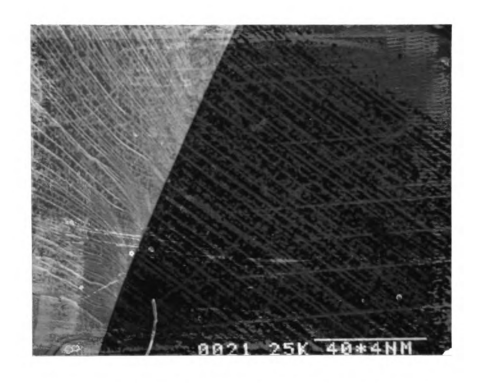
0: 85°
Twist(\$): 7°
Tilt: 45°
Magnification: 100X(SEM)
Specimen number: 11

Figure 22. Uniform distribution of dislocation etch pits.



8: 86⁰
Twist(\$): 7⁰
Tilt: 45⁰
Magnification: 350X(SEM)
Specimen number: 12

Figure 23. Uniform distribution of dislocation etch pits.



6: 90°
Twist(\$\phi\$): 45°
Tilt: 45°
Magnification: 75X(SEM)
Specimen number: 20

Figure 24. Uniform distribution of dislocation etch pits.

6 DISCUSSION

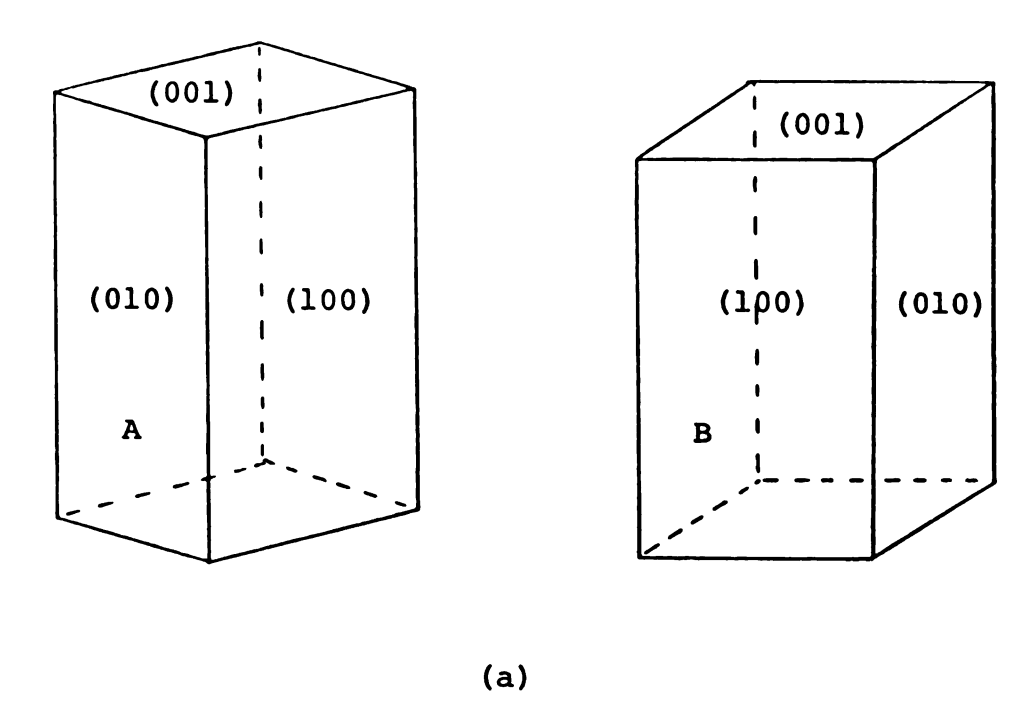
6.1 Seed Setting

In order to make the intersected lines of cleavage planes of crystal A and B parallel to the [001] direction, two different arrangements of seeds can be used as shown in figure 25, 26. If the seeds with [100] growth direction are arranged to be parallel to each other as shown in figure 25, the maximum misorientation angle is 45° because there exists two primary cleavage planes i.e., (100) and (010) planes in crystal B. Thus, to grow the bicrystals having large misorientation angles (>45°), two seeds were set as shown in figure 26. To change the misorientation angles, one seed was rotated keeping its (001) plane to remain perpendicular to crystal growth direction. Thus, the grain boundaries of the bicrystals grown by such seed setting have twist character and tilt character. The range of twist angle is 0° to 90°, whereas the tilt angle is 45°.

Based on crystal structure of LiF and seed setting, the bicrystals grown have one primary cleavage plane, (100), and one secondary cleavage plane, (011), along which crack could propagate in grain B when crack reaches the boundary in grain A by (100) cleavage.

6.2 Specimen Geometry

Most quantitative treatments of fracture are based on the Griffith criteria,



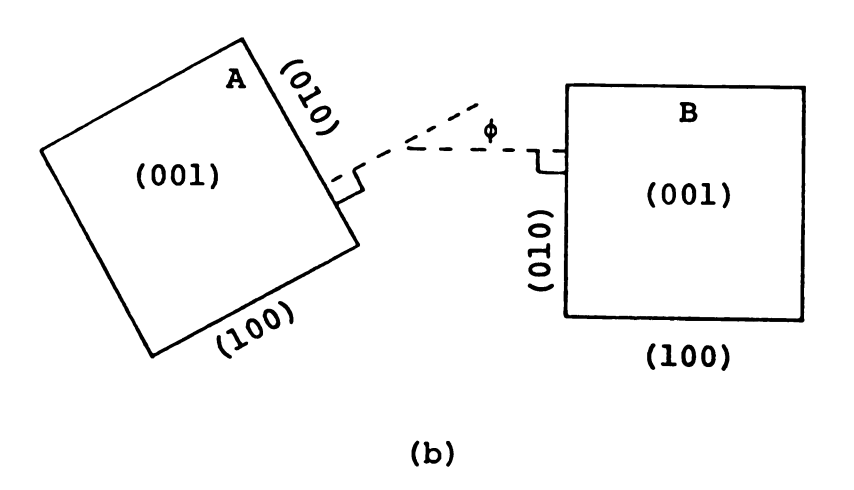
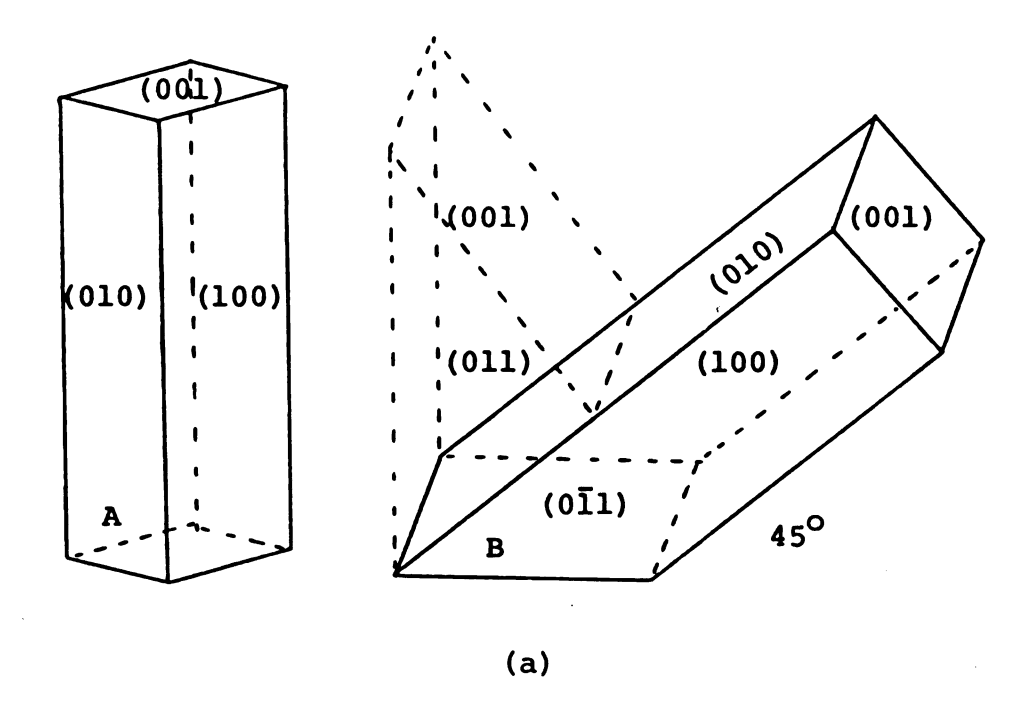


Figure 25. Parallel seed setting (tilt: 0° , twist: ϕ)

(a) Schematic drawing

(b) Top view



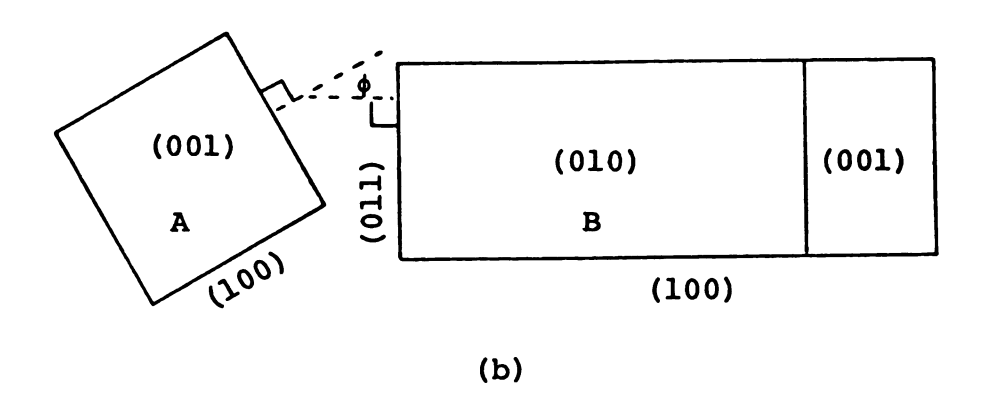


Figure 26. 45° slant seed setting
(tilt: 45°, twist: φ)
(a) Schematic drawing

(b) Top view

$$\sigma = \left(\frac{2E\gamma_{S}}{\pi a}\right)^{\frac{1}{2}} \tag{12}$$

where σ is the stress at fracture, E is the elastic modulus, γ_s is the "surface energy", and 'a' is the crack length. But, this equation can be applied only for ideally brittle, linear elastic fracture.

Irwin took the approach that the surface energy should be replaced by a strain energy release rate, $G_{\rm C}$, hence

$$\sigma = \left(\frac{EG_C}{\pi a}\right)^{\frac{1}{2}} \tag{13}$$

which includes all the energies involved in fracture, both elastic and inelastic.

In determining G_C using double cantilever beams (DCB) the fracture energy is equated to the strain energy at crack initiation. Assuming that the specimen responds elastically (except at the crack tip)

$$G_{C} = \frac{1}{2} \frac{P_{C}^{2}}{2b} \frac{dc}{da}$$
 (14)

where 'b' is the specimen width and 'dc/da is the change in the compliance of the specimen with crack length. In the case of a DCB, equation (14) becomes

$$G_{c} = \frac{4P_{c}^{2}}{b^{2}E_{b}} \left(\frac{3a^{2}}{h^{3}} + \frac{1}{h}\right)$$
 (15)

where 'h' is the beam height and E_{h} is the bending modulus.

Mostovoy designed a tapered double cantilever beam specimen such that 'dc/da' is a constant, 'm', over the length of the specimen, and equation (15) becomes

$$G_{c} = \frac{4P_{c}^{2}}{b^{2}E_{b}} m$$
 (16)

The taper is determined by the bracketed term in equation (15) [28, 29, 30]. The advantages of this specimen is that $G_{\rm c}$ is given by the load, $P_{\rm c}$, without any need to measure crack length. Also, this specimen design allows the crack to propagate at constant velocity for a constant rate of separation unless the fracture energy is a function of crack speed. Also stress is relatively insensible to crack length for this specimen geometry.

6.3 Direction of Crack Propagation

The brittle fracture of single crystal is considered to be related to the resolved normal stress on the cleavage plane. Fracture occurs when the resolved normal stress reaches a critical value. The component of the tensile force which acts normal to the cleavage plane is P cos \$\phi\$ where P is external load and \$\phi\$ is the angle between the tensile axis and the normal to the plane. The area of the cleavage plane is A/cos \$\phi\$ where A is the cross-sectional area normal to the tensile axis. Therefore, the critical normal stress for brittle fracture is

$$\sigma_{\rm C} = \frac{P \cos \phi}{A/\cos \phi} = \frac{P}{A}\cos^2 \phi \qquad (17)$$

Most brittle fractures occur in a transcrystalline manner. However, if the grain boundaries contain a film of brittle constituent, the fracture will occur in an intercrystalline manner. The grain boundary weakness is an intrinsic characteristic of nonmetallic substances, so intercrystalline fracture could also happen in a very pure specimen. The critical normal stress is related to the surface energies of the cleavage planes and grain boundary. Thus, depending upon the relative crystallographic and grain boundary orientations, and according to the conditions of stress concentration, the direction of crack propagation is decided.

The effective surface energy (γ_s) was determined by the following method [31]. Notched single crystal and bicrystal specimens were fractured in three point bending. Values of the fracture stress (σ_F) , the notch depths (c), and the elastic modulus (E) as determined from the notched-bar three-point bending test, were used to obtain the effective fracture surface energy.

When the notch depth(c) is small compared with the beam depth, the effective surface energy(γ_S) is given by Irwin and Orowan as

$$\gamma_{s} = \frac{(1-v^2)\pi\sigma_{F}c}{2F} \tag{18}$$

where, ν is Poissons ratio, E is Young's modulus, and $\sigma_{\rm F}$ is the fracture stress, $\sigma_{\rm F}$ is given by

$$\sigma_{\mathbf{F}} = \frac{3}{2} P_{\mathbf{f}} \frac{1}{\mathbf{b} d^2} \tag{19}$$

where, P_f is fracture load, 'b' is breadth, 'l' is span, and 'd' is the specimen thickness. The specimen geometry is given in figure 27. The experimental values of the surface energy are listed in table 4. From Hooke's law, the following relation is derived.

$$\sigma_{\text{th}} = \sqrt{\frac{E\gamma}{a_0}}$$
 (20)

where σ_{th} = theoretical strength for fracture

E = Young's modulus

γ = surface energy

a = lattice constant

By substituting the constants of LiF (E=10.2 x 10^{11} dyn/cm², $a_{\rm o} = 4.027$ x 10^{-8} cm) to the above equation, the theoretical strength needed for separation is calculated. The values are listed in table 5. Intercrystalline fracture happens when $\sigma_{\rm c} > \sigma_{\rm gb}$, and transcrystalline fracture happens when $\sigma_{\rm c} > \sigma_{\rm cpl}$ or $\sigma_{\rm c} > \sigma_{\rm cp2}$ depending upon the relative crystallographic and grain boundary orientations.

When a crack tip approaches the grain boundary, crack propagation can occur by one of the following four modes:

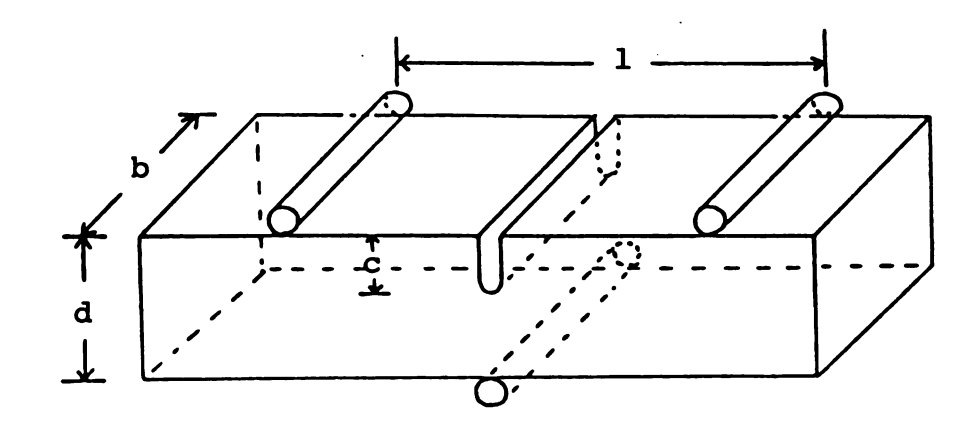


Figure 27. Specimen geometry for three point bending test to determine fracture surface energy.

Table 4. Experimental values of surface energy

γ _{cpl} (surface energy of {001} plane)	520 ergs/cm ²
γ _{cp2} (surface energy of {011} plane)	2,000 ergs/cm ²
γ _{gb} (average grain boundary energy)	940 ergs/cm ²

Table 5. Calculated values of theoretical strength

σ _{cpl} (primary cleavage plane)	1.15 x 10 ¹¹ dyn/cm ²
σ _{cp2} (secondary cleavage plane)	2.25 x 10 ¹¹ dyn/cm ²
σ _{gb} (grain boundary)	1.54 x 10 ¹¹ dyn/cm ²

intercrystalline fracture, transcrystalline fracture along the primary cleavage plane, transcrystalline fracture along the secondary cleavage plane, or fracture along the secondary cleavage plane existing in the crystal containing intial crack.

If tensile stress σ_g is applied on the crack tip at grain boundary of a bicrystal, theoretical strengthes and the resolved normal stresses are equal at the critical point (just before the crack propagation).

$$\sigma_{\rm cpl} = \sigma_{\rm q} \cos^2 \phi \tag{21}$$

$$\sigma_{\rm CD2} = \sigma_{\rm g} \cos^2(90^{\rm O} - \phi) \tag{22}$$

$$\sigma_{\rm qb} = \sigma_{\rm q} \cos^2 \theta \tag{23}$$

$$\sigma_{\text{cp2.A}} = \sigma_{\text{g}} \cos^2 45^{\circ} \qquad (24)$$

From the results of experiment (table 5)

$$\sigma_{\rm cpl} = 0.746 \, \sigma_{\rm gb} \tag{25}$$

$$\sigma_{cp2} = 1.461 \sigma_{qb} \tag{26}$$

$$\sigma_{\rm cpl} = 0.511 \, \sigma_{\rm cp2} \tag{27}$$

$$\sigma_{\text{cp2.A}} = 1.461 \, \sigma_{\text{gb}} \qquad (28)$$

By crystal structure, the angle between (100) plane and the secondary cleavage plane ($1\overline{1}0$) in crystal A is 45° as shown in equation (24). From the equations (23), (24) and (28)

$$\sigma_{\rm q} \cos^2 45^{\rm O} = 1.461 \, \sigma_{\rm q} \cos^2 \theta$$
 . (29)

Thus, crack propagation along the secondary cleavage plane existing in crystal A occurs when $\theta > 54.2^{\circ}$. But, if $\theta > 54.2^{\circ}$ erystal A does not contain (110) plane in the direction of

crack propagation. Therefore, such crack propagation is impossible to occur.

From the equation (21), (23) and (25) the condition for transcrystalline fracture along the primary cleavage plane is $\cos^2 \phi < 0.7437 \cos^2 \theta$ and the condition for intercrystalline fracture is $\cos^2 \phi > 0.7437 \cos^2 \theta$. these conditions are shown in figure 28.

Likewise, from the equation (22), (23) and (26) the condition for transcrystalline fracture along the secondary cleavage plane is

$$\sigma_{q} \cos^{2} (90^{\circ} - \phi) < 1.461 \sigma_{q} \cos^{2} \theta$$
 (30)

and the condition for intercrystalline fracture is

$$\sigma_{g} \cos^{2} (90^{\circ} - \phi) > 1.461 \sigma_{g} \cos^{2} \theta$$
 (31)

These conditions are shown in figure 29. The orientation of grain boundary does not have any effect on the cleavage direction along the primary cleavage plane or secondary cleavage plane. So, from the equations (21), (22) and (27) the condition for crack propagation along the primary cleavage plane is $\cos^2\phi > 0.511\cos^2(90^{\circ}-\phi)$ and that for secondary cleavage plane is $\cos^2\phi < 0.511\cos^2(90^{\circ}-\phi)$. These conditions are shown in figure 30. Thus, by superimposing the crack propagation conditions shown in figure 28, 29 and 30 the angular conditions for different

crack propagation modes is shown in figure 31.

The curve of figure 28 shows the various combinations of critical angles (θ and ϕ) at which intercrystalline fracture and transcrystalline cleavage along the primary cleavage plane could occur simultaneously.

The curve of figure 29 shows the various combinations of critical angles (θ and ϕ) at which intercrystalline fracture and transcrystalline cleavage along the secondary cleavage plane could occur simultaneously. The critical value of ϕ is 54.5° at which transcrystalline cleavage could occur along the primary cleavage plane or secondary cleavage plane.

Thus, in the zone 'TR.1.' in figure 31, only transcrystalline cleavage (along the primary cleavage plane) could occur. And, in the zone 'TR.2' in figure 31, only transcrystalline cleavage (along the secondary cleavage plane) could occur. In the zone 'IN.' in figure 31, only intercrystalline fracture occurs. But at the critical point which is the junction of three curves, the three possible modes of crack propagation could occur simultaneously.

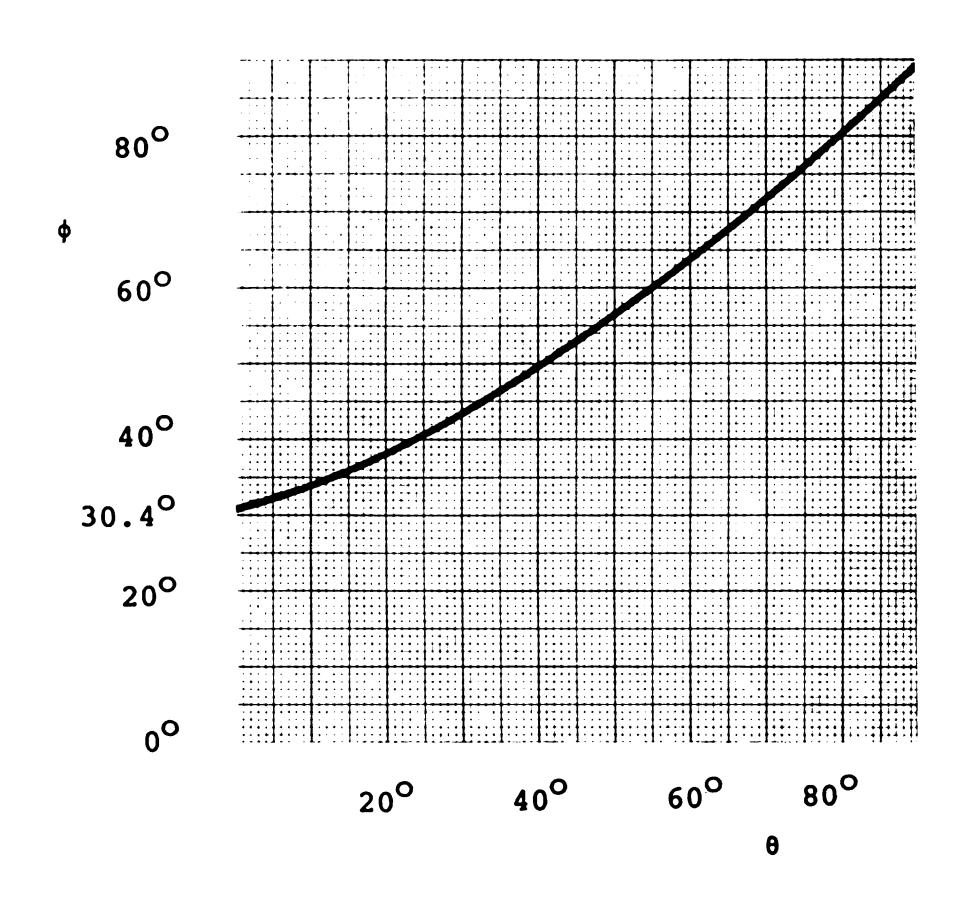


Figure 28. Locus of critical angles for intercrystalline fracture and primary cleavage.

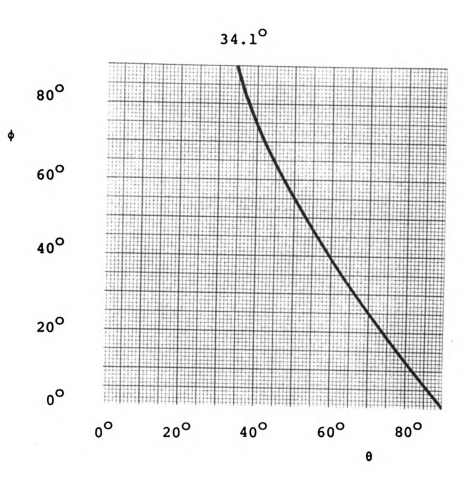


Figure 29. Locus of critical angles for intercrystalline fracture and secondary cleavage.

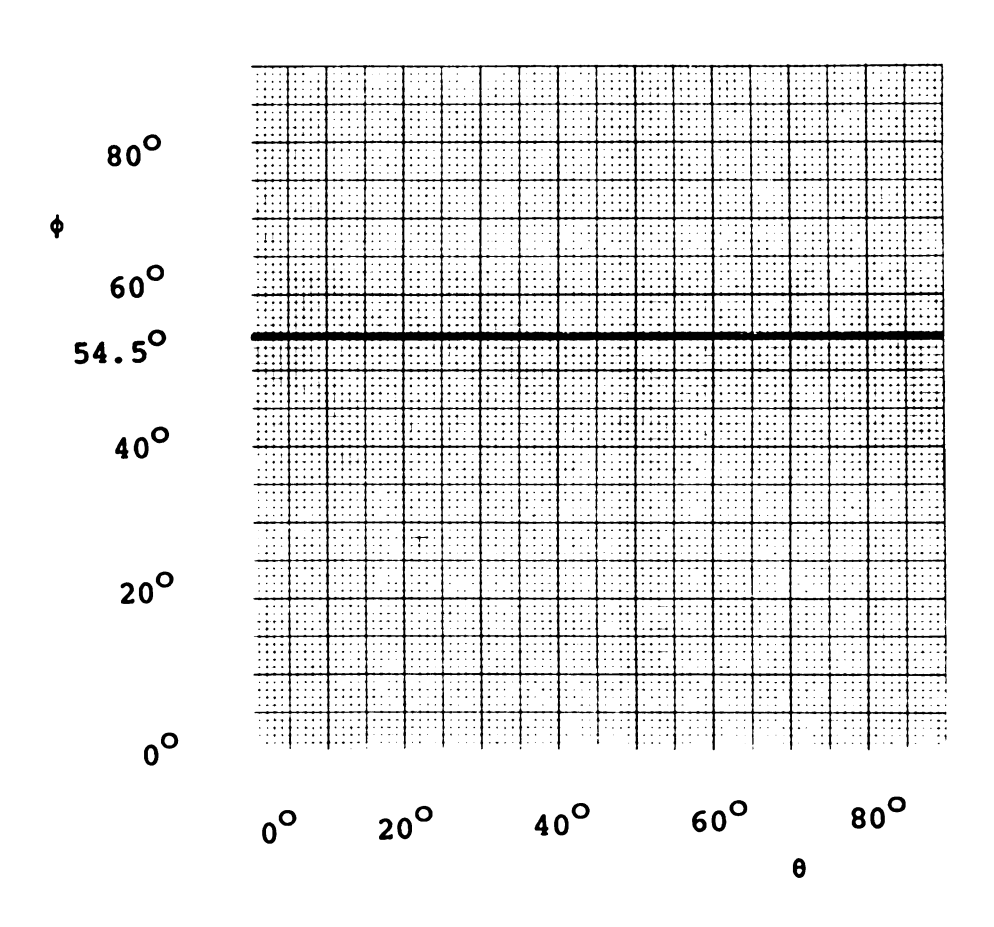


Figure 30. Locus of critical angles for primary cleavage and secondary cleavage.



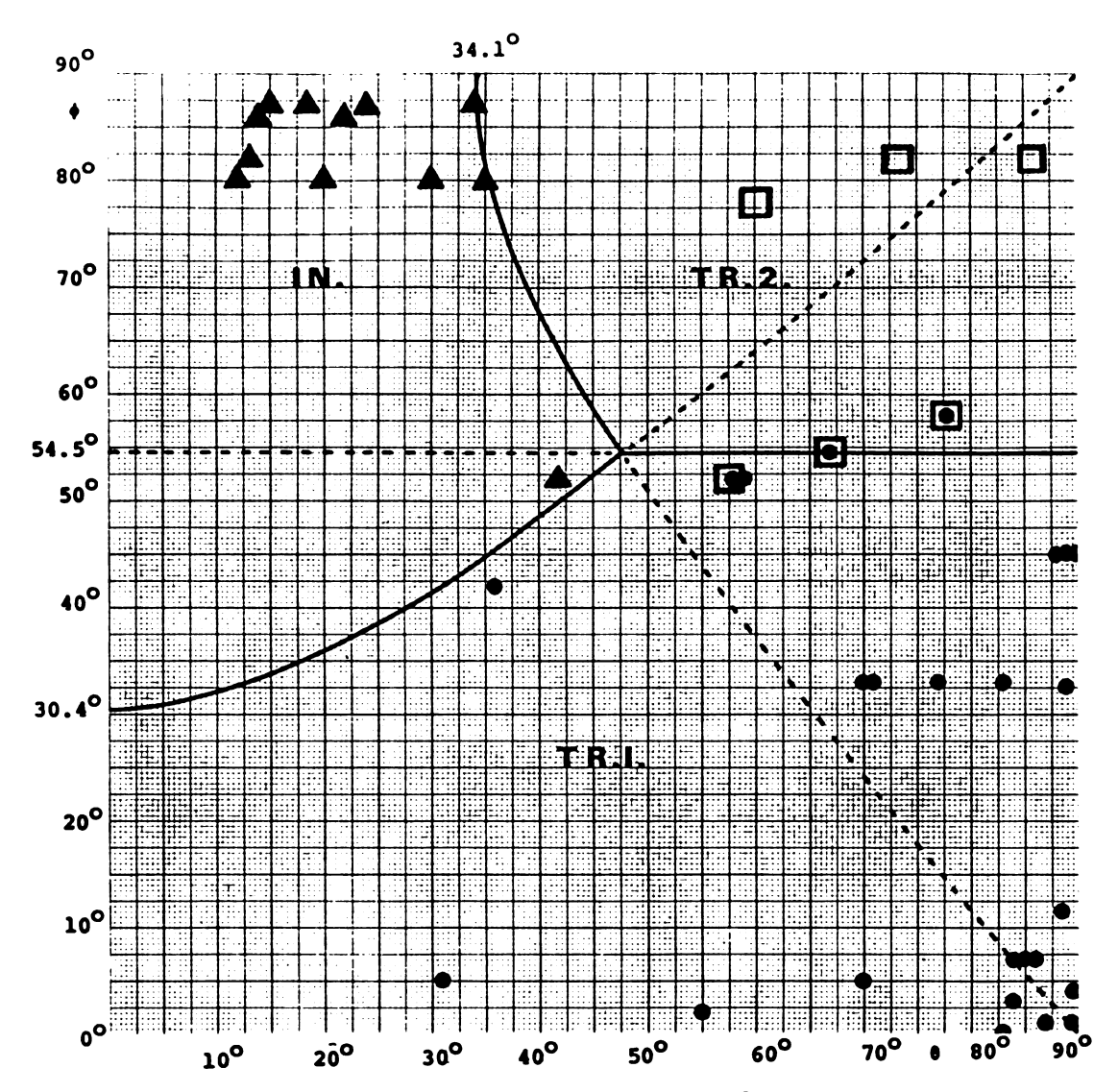


Figure 31. Crack propagation mode for various 0 and 0.

Experimental points are indicated in the same plot.

- ▲ intercrystalline fracture
- transcrystalline(primary) cleavage
- transcrystalline(secondary) cleavage
- IN intercrystalline propagation zone
- TR.1. transcrystalline(primary) propagation zone
- TR.2. transcrystalline(secondary) propagation zone

6.4 Relation Between Fracture Load and Misoeientation
Angles

In the case of intercrystalline crack propagation, fracture load is a function of θ values. To find out the relation between fracture loads and θ values, some experimental results are presented in table 6 and 7. The compared values are the ones having similar ϕ values. Likewise, in the case of transcrystalline crack propagation, fracture load is a function ϕ values. Some experimental results are also selected and compared in tables 8 and 9. The corresponding θ values are similar.

The relations between fracture loads and θ are shown in figure 32 and 33. From the curves, fracture load for intercrystalline fracture increases as the angle θ increases. Likewise, from the curves shown in figure 34 and 35, fracture load for transcrystalline fracture increases as the misorientation angle ϕ increases.

As the fracture paths changed depending upon the relative crystallographic orientations, the fracture loads were also changed according to the relative crystallographic and grain boundary orientations.

6-5 Dislocation Etch Pit Studies

Based on the specimen geometry, crack can be regarded propagate at constant velocity for a constant rate of separation. But, at grain boundary, the crack tip should change the direction of crack propagation and should accommodate the crack propagation to neighbouring crystal.

Therefore, the velocity of crack propagation should be slowed down.

According to Gilman [12], the number of dislocations caused by the crack decreases as its velocity increases, and approaches zero at high velocities. In the case of bicrystals having small misorientation angles shown in figure 21 to 24, the distribution of dislocation etch pits are uniform because the velocity change of crack tip is small, and it appears this is still above the critical velocity for dislocation. Even in the case of bicrystals having large misorientation angles, shown in figure 24, the distribution of dislocation etch pits is also uniform. Thus, the amount of velocity change of crack tip near grain boundary seems to be similar from specimen to specimen even though the misorientation angles were different. The main reason of the similar change of speed seems to be the special specimen geometry.

Table 6. Comparison of fracture load with θ values. $(86^{\circ} \le \phi \le 87^{\circ}, \text{ intercrystalline fracture})$

θ	fracture load(kg)	ф	specimen number
14	9.57	86	36
18.5	22.33	87	39
22	35.09	86	37
24	43.06	87	38
34	39.87	87	40

Table 7. Comparison of fracture load with θ values. $(80^{\circ} \le \phi \le 82^{\circ}, \text{ intercrystalline fracture})$

θ	fracture load(kg)	ф	specimen number
12	20.73	80	29
13	28.71	82	33
20	30.30	80	30
30	49.44	80	31
35	87.72	80	32

Table 8. Comparison of fracture load with ϕ values. $(86^{\circ} \le \theta \le 90^{\circ}, \text{ transcrystalline fracture})$

ф	fracture load(kg)	θ	specimen number
1	19.14	89.5	2
4	22.33	89.5	7
7	22.33	86	12
11.5	19.14	88.5	13
33	30.30	89	15
45	47.85	88	21

Table 9. Comparison of fracture load with ϕ values. $(83^{\circ} \leq \theta \leq 85^{\circ}, \text{ transcrystalline fracture})$

ф	fracture load(kg)	θ	specimen number
0	25.52	83	1
3	15.95	84	6
7	15.95	84	10
7	22.33	8.5	11
33	33.49	83	14

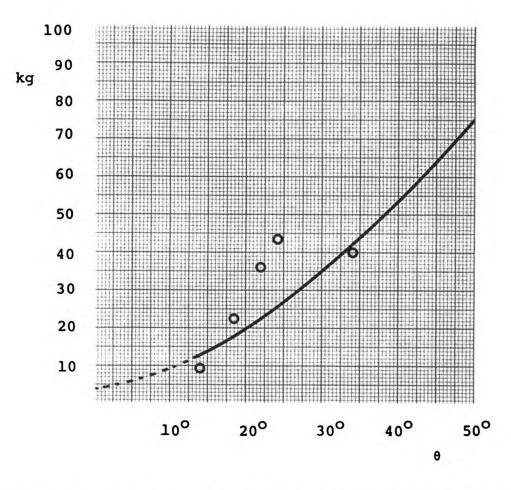


Figure 32. Relation between fracture load and θ values. $(86^{\rm O} \, \leq \, \varphi \, \leq \, 87^{\rm O})$

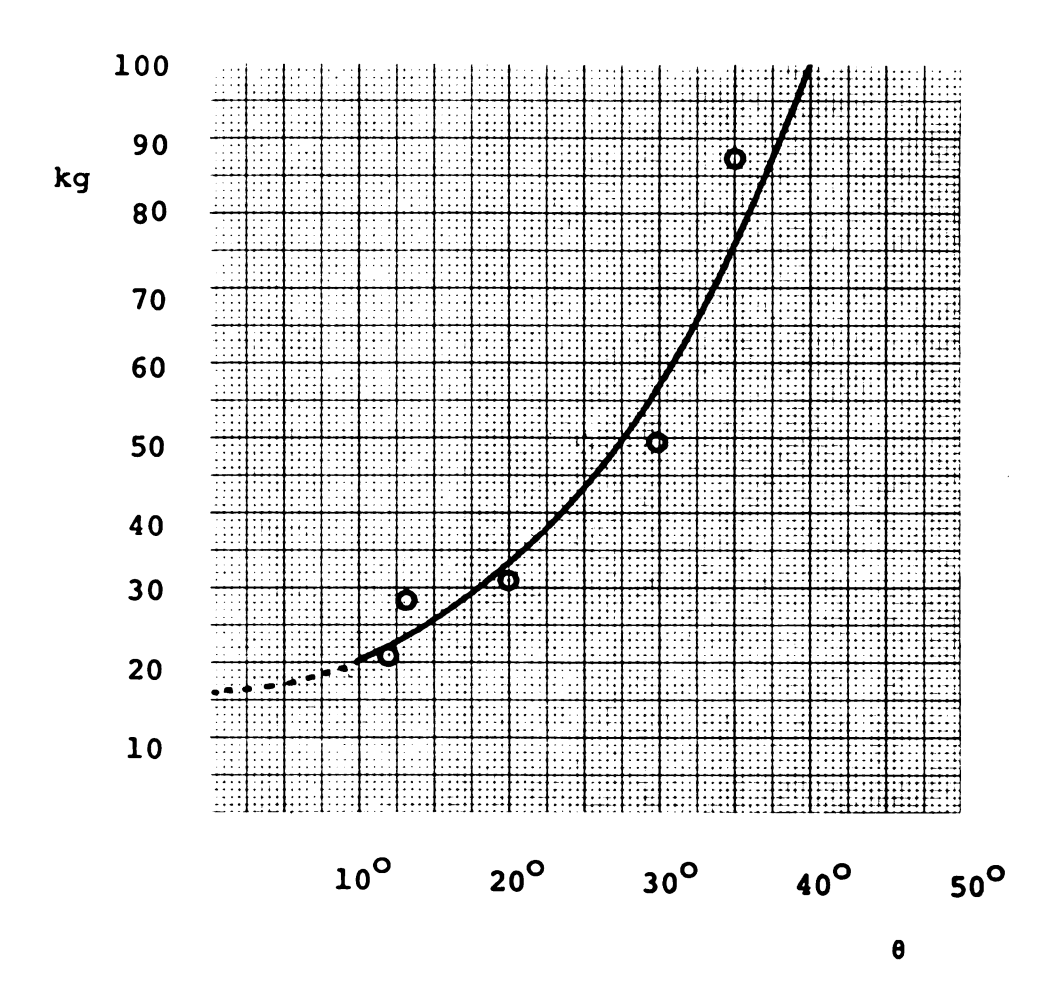


Figure 33. Relation between fracture load and 0 values. $(80^{\circ} \le \phi \le 82^{\circ})$

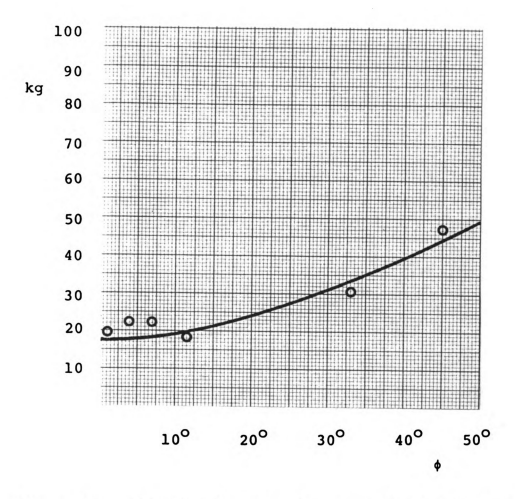


Figure 34. Relation between fracture load and ϕ values. $(86^{O} \, \leq \, \theta \, \leq \, 90^{O})$

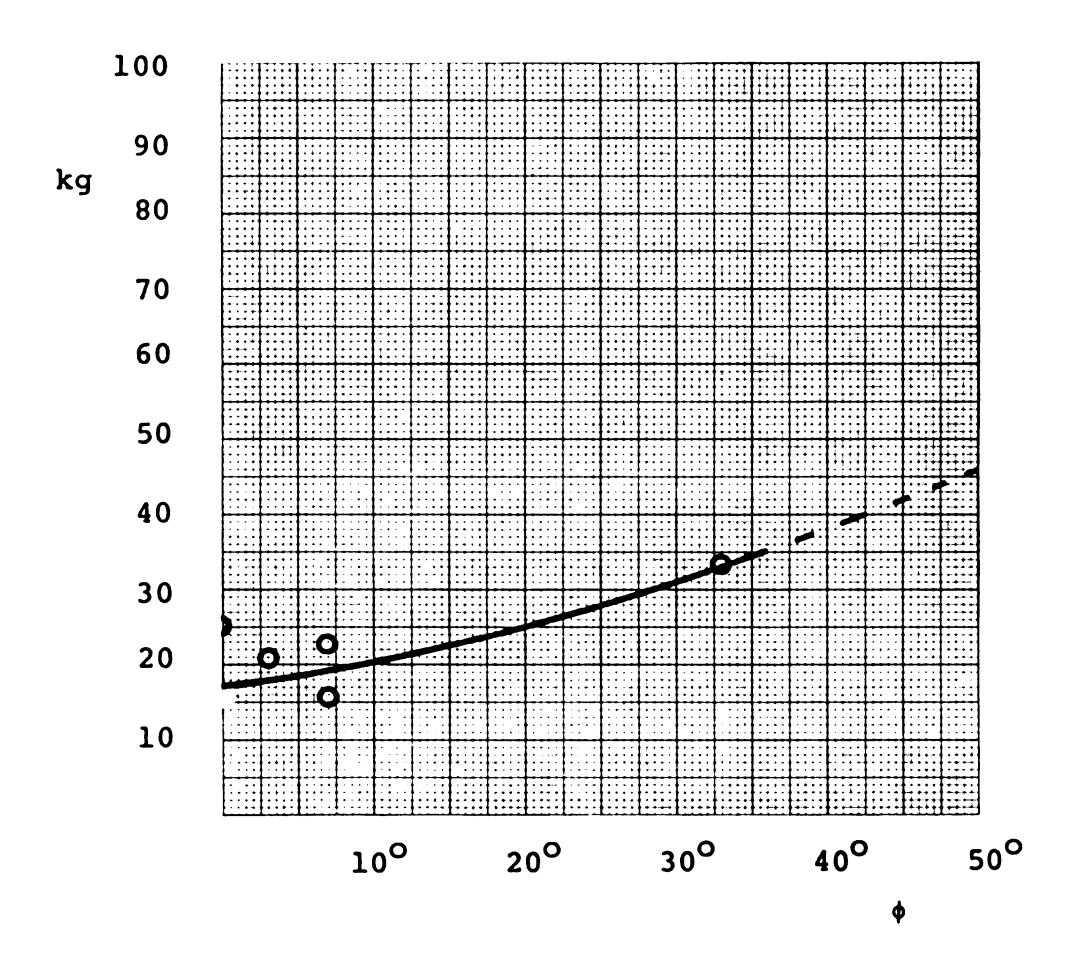


Figure 35. Relation between fracture load and ϕ values. $(83^{\circ} \le \theta \le 85^{\circ})$

7 CONCLUSIONS

- 1. Grain boundaries of bicrystals are found to be extremely effective barriers to the crack propagation as evidenced by the larger load required to fracture bicrystals (compared to single crystals).
- 2. Crack paths changed at the grain boundary according to the crystallographic orientation of the adjacent grain and grain boundary orientation relative to the crack path.
- 3. When the twist angle(ϕ) was smaller than 30.4°, only primary cleavage fracture occurred regardless of the value of the angle of relative grain boundary orientation(θ). Similarly for values of θ ranging from 47.6° to 90°, primary cleavage always occurred provided ϕ is below 54.5°. For the values of θ ranging from 0° to 47.6°, primary cleavage occurred provided ϕ is smaller than the corresponding critical angles, ranging from 30.4° to 54.5°.
- 4. At room temperature, secondary cleavage fracture is initiated when the twist angle(ϕ) is larger than 54.5° and grain boundary is oriented at $\theta \ge 47.6^{\circ}$ with respect to crack plane. This condition persists for smaller values of θ as long as the ϕ values are larger than the corresponding critical ϕ values.

- 5. When the twist angle(ϕ) was larger than the critical angles, intercrystalline fracture also happened provided θ value was smaller than the critical angle at which intercrystalline fracture and secondary cleavage can occur simultaneously.
- 6. Intercrystalline and transcrystalline fracture or primary and secondary cleavage fracture happened simultaneously at the critical angles.
- 7. Fracture loads were increased when the misorientation angles increased.
- 8. As the crack propagates through a grain boundary, it produces cleavage steps in adjoining grain. The density and height of these cleavage steps seem to depend on the twist angle of the boundary.
- 9. Although the relative crystallographic misorientation angles are different from specimen to specimen, the crack front speed decreases slightly as it approaches the grain boundary as is evidenced by the uniform density of dislocation etch pits throught the fracture surfaces.

REFERENCES

- 1. Gilman, J. J., "Plastic Anisotropy of Lithium Fluoride and Other Rock-salt Type Crystals," Acta. Met., 7, p 608, (1959).
- Hulse, C. O., Copley, S. M. and Pask, J. A., "Effect of Crystal Orientation on the Plastic Deformation of MgO," J. Am. Ceram. Soc., 46, p 317, (1963).
- 3. Gilman, J. J., Knudsen, C. and Walsh, W. P., "Cleavage Cracks and Dislocations in LiF Crystals," J. Appl. Phys., 29, p 601, (1958).
- 4. Mott, N. F., "Fracture of Metals: Theoretical Considerations," Engineering, 165, p 16, (1948).
- 5. Roberts, D. K. and Wells A. A., "The Velocity of Brittle Fracture: Terminal Velocity Related to Elastic-Wave Velocity," Engineering, 178, p 820, (1954).
- 6. Lawrence Bragg, F. R. S. and Nye, J. F., "A Dynamical Model of a Crystal Structure," Proc. Roy. Soc. <u>A 190</u>, p 474, (1947).
- 7. Cottrell, A. H., "Theory of Brittle Fracture in Steel and Similar Metals," Trans. Met. Soc. AIME, 212, p 192, (1958).
- 8. Washburn, J., Gorum, A. E. and Parker, E. R., "Cause of Cleavage Fractures in Ductile Materials," Trans. Met. Soc. AIME, 215, p 230, (1959).
- 9. Stokes, R. J., Johnston, T. L. and Li, C. H., "The Relationship between Plastic Flow and the Fracture Mechanism in Magnesium Oxide Single Crystals," Phil. Mag., 4, p 920, (1959).
- 10. Takasugi, T., Izumi, O. and Halla, N. B., "Transgranular Slip and Fracture across an Interface in

REFERENCES

- Alpha/Beta Brass Two-phase Bicrystals," J. Materials Sci., 15, p 945, (1980).
- 11. Keh, A. S., Lì, J. C. M. and Chou, Y. T., "Cracks due to the Piling-up of Dislocations on two Intersecting Slip Planes in MgO Crystals," Acta. Met., 7, p 694, (1959).
- 12. Gilman, J. J., "Creation of Cleavage Steps by Dislocation," Trans. Met. Soc. AIME, 212, p 310, (1958).
- 13. Gilman, J. J., "Reduction of Cohesion in Ionic Crystals by Dislocations," J. Appl. Phys., 32, p 738, (1961).
- 14. Gilman, J. J., "Deformation of Symmetric Zinc Bicrystals," Acta. Met., 1, p 426, (1953).
- 15. Clark, R. and Chalmers, B., "Mechanical Deformation of Aluminum Bicrystals," Acta. Met., 2, p 80, (1954).
- 16. Aust, K. T. and Chen, N. K., "Effect of Orientation Difference on the Plastic Deformation of Aluminum Bicrystals," Acta. Met., 2, p 632, (1954).
- 17. Livingston, J. D. and Chalmers, B., "Multiple Slip in Bicrystal Deformation," Acta. Met., 5, p 322, (1957).
- 18. Hauser, J. J. and Chalmers, B., "The Plastic Deformation of Bicrystals of F. C. C. Metals," Acta. Met., 9, p 802, (1961).
- 19. Koppenaal, T. J., "Slip Lines across an f.c.c.-b.c.c. Interface," Acta. Met., 10, p 684, (1962).
- 20. Davis, K. G. and Teghtsoonian, E. and Lu, A., "Slip Band Continuity across Grain Boundaries in Aluminum," Acta. Met., 14, p 1677, (1966).
- 21. Hook, R. E. and Hirth, J. P., "The Deformation Behavior of Isoaxial Bicrystals of Fe-3% Si," Acta. Met., 15,

REFERENCES

- p 535, (1967).
- 22. Sadananda, K. and Marcinkowski, M. J., "Deformation of Internal Boundaries," J. Materials Sci., 9, p245, (1974).
- 23. Sadananda, K. and Marcinkowski, M. J., "Mutual Annihilation of Unlike Dislocations by Cross Slip in Ordered and Disordered Alloys," J. Appl. Phys., 44, p 4445, (1973).
- 24. Westwood, A. R. C., "On the Fracture Behavior of MgO Bicrystals," Phil. Mag., 6, p 195, (1961).
- 25. Johnston, T. L., Stokes, R. J. and Li, C. H., "Crack Nucleation in Magnesium Oxide Bi-crystals Under Compression," Phil. Mag., 7, p 23, (1962).
- 26. Subramanian, K. N., "Work Hardening and Deformation Structure in Lithium Fluoride Single Crystals," Ph. D. Thesis, Michigan State Univ., (1966).
- 27. Gilman, J. J., "Direct Measurement of the Surface Energies of Crystals," J. Appl. Phys., 31, p 2208, (1960).
- 28. Bascom, W. D., Cottington, R. L., Jones, R. L. and Peyser, P., "The Fracture of Eposy-and Elastomer-Modified Epoxy Polymers in Bulk and as Adhesives," J. Applied Polymer Science, 19, p 2545, (1975).
- 29. Srawley, J. E. and Gross, B., "Stress Intensity Factor for Crackline Loaded Edge-Crack Specimens," Materials Research & Standards, p 155, (1967).
- 30. Mai, Y. W., Atkins, A. G. and Caddell, R. M., "On the Stability of Cracking in Tapered DCB test pieces," Int. J. of Fracture, 11, p 939, (1975).
- 31. Davidge, R. W. and Tappin, G. "The Effective Surface Energy of Brittle Materials," J. Materials Sci., 3, p 165, (1968).